ansa-Chromocene Complexes. 2. Isocyanide Derivatives of Cr(II) and Cr(III), Their Syntheses, X-ray Crystal Structures, and Physical Properties

Pamela J. Shapiro,*,† Ralph Zehnder,†,‡ David M. Foo,† Philippe Perrotin,† Peter H. M. Budzelaar,§ Sharon Leitch,† and Brendan Twamley†

Departments of Chemistry, University of Idaho, Moscow, Idaho 83844-2343, and University of Manitoba, Winnipeg, Manitoba R3T 2N2, Canada

Received August 17, 2005

A variety of 18*e ansa*-chromocene isocyanide complexes were prepared via ligand substitution on the carbonyl complexes. The relative π-accepting character of the different isocyanide ligands was evaluated from the structural, spectroscopic, and electrochemical properties of the complexes. One-electron chemical oxidation of the complexes generates low-spin, 17*e ansa*-chromocene isocyanide cations, the structural and spectroscopic properties of which were compared with their neutral precursors. Density functional theory (DFT) calculations were performed on model complexes in order to elucidate the nature of the bonding between the chromium and the isocyanide ligands and to explain the effects of one-electron oxidation of the complexes.

Introduction

Isocyanide ligands are often interchangeable with CO in transition metal complexes, although they are, in general, better σ-donors and poorer π-acceptors than CO.[1,2] They are also similar to CO in their usefulness for probing the electron-donating/accepting properties of the metal, which is manifested in the energy of the C−N stretching vibration, the bond angle about nitrogen, and the ^{13}C and ^{15}N NMR chemical shifts of the ligands.[3,4] Isocyanide ligands are more versatile ligands than CO in the sense that the substituent on nitrogen can be varied to influence the donor/acceptor properties of the ligand and to manipulate the architectures of metal complexes that are constructed with the ligand. For example, bridging diisocyanide ligands have been used to support a variety of dinuclear metal−metal bonded species[5−10] as well as metal-containing macrocycles and polymers.[10−17]

In our efforts to explore the reactivity of bent-sandwich chromocene complexes we have found isocyanide ligands to be useful alternatives to CO for stabilizing 16*e ansa*-chromocene fragments, which are destabilized relative to parent Cp_2Cr by the enforced bending of the cyclopentadienyl rings by the *ansa*-bridge.[18] Schwemlein et al. recognized the need to trap the *ansa*-chromocene as it formed in situ in their synthesis of the complex $Me_4C_2(C_5H_4)_2CrCO$.[19] In the absence of CO, an ill-defined, THF-insoluble, brick-red material is obtained instead. We later found that *tert*-butyl isocyanide could be used instead of CO to form the corresponding 18*e ansa*-chromocene isocyanide derivative according to the reaction shown in eq 1.[20,21]

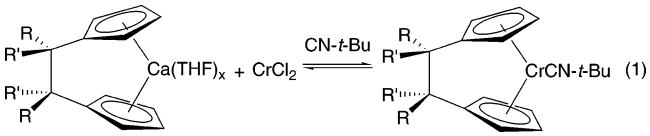

Other isocyanide ligands are unsuccessful at trapping the *ansa*-chromocene fragment, affording only insoluble, brick-red materials. A more general approach to isocyanide derivatives involves reversible ligand substitution on the carbonyl species.

* Corresponding author. E-mail: shapiro@uidaho.edu.
† University of Idaho.
‡ Current address: Department of Chemistry, University of Louisiana at Monroe, Monroe, LA 71209.
§ University of Manitoba.

(1) Trechel, P. M. In *Adv. Organomet. Chem*; Stone, F. G. A., West, R., Eds.; Academic Press: New York, 1973; Vol. 11, pp 21−81.
(2) Singleton, E.; Oosthuizen, H. In *Adv. Organomet. Chem*; Stone, F. G. A., West, R., Eds.; Academic Press: New York, 1983; Vol. 22, pp 209−310.
(3) Becker, W.; Beck, W.; Rieck, R. *Z. Naturforsch.* **1970**, *25b*, 1332−1337.
(4) Guy, M. P.; Coffer, J. L.; Rommel, J. S.; Bennett, D. W. *Inorg. Chem.* **1988**, *27*, 2942−2945.
(5) Bartolomaes, T.; Lentz, D.; Neubert, I.; Roettger, M. *Z. Anorg. Allg. Chem.* **2002**, *628*, 863−871.
(6) Mixa, M. M.; Sykes, A.; Mann, K. R. *Inorg. Chim. Acta* **1989**, *160*, 159−65.
(7) Ohtani, Y.; Miya, S.; Yamamoto, Y.; Hiroshi, Y. *Inorg. Chim. Acta* **1981**, *53*, L53−L55.
(8) Dartiguinave, M.; Dartiguinave, Y.; Guitard, A.; Mari, A. *Polyhedron* **1989**, *8*, 317−323.
(9) Harvey, P. D. *Coord. Chem. Rev.* **2001**, *219*−*221*, 17−52.
(10) Siemeling, U.; Rother, D.; Ruhr, C.; Fink, H.; Weidner, T.; Träger, F.; Rothenberger, A.; Fenske, D.; Priebe, A.; Maurer, J.; Winter, R. *J. Am. Chem. Soc.* **2005**, *127*, 1102−1103.
(11) MacDonald, M.; Puddephatt, R. J. *Organometallics* **2000**, *19*, 2194−2199.
(12) Irwin, M. J.; Jia, G.; Vittal, J. J.; Puddephatt, R. J. *Organometallics* **1996**, *15*, 5321−5329.
(13) Su, Z. M.; Wang, R. S.; Che, C.-M. *Mater. Res. Soc. Symp. Proc.* **1999**, *576*, 389−394.
(14) Hanack, M.; Deger, S.; Lange, A. *Coord. Chem. Rev.* **1988**, *83*, 115−136.
(15) Feinstein-Jaffe, I.; Maisuls, S. E. *J. Organomet. Chem.* **1988**, *350*, 57−75.
(16) Schroelkamp, S.; Sperber, W.; Lentz, D.; Fehlhammer, W. P. *Chem. Ber.* **1994**, *127*, 621−629.
(17) Fournier, E.; Sicard, S.; Decken, A.; Harvey, P. D. *Inorg. Chem.* **2004**, *43*, 1491−1501.
(18) Green, J. C.; Jardine, C. N. *J. Chem. Soc., Dalton Trans.* **1999**, 3767−3770.
(19) Schwemlein, H.; Zsolnai, L.; Huttner, G.; Brintzinger, H.-H. *J. Organomet. Chem.* **1983**, *256*, 285−289.
(20) Foo, D. M. J.; Shapiro, P. J. *Organometallics* **1995**, *14*, 4957−4959.
(21) Matare, G. J.; Foo, D. M.; Kane, K. M.; Zehnder, R.; Wagener, M.; Shapiro, P. J. *Organometallics* **2000**, *19*, 1534−1539.

10.1021/om050710j CCC: $33.50
Publication on Web 01/05/2006

Scheme 1

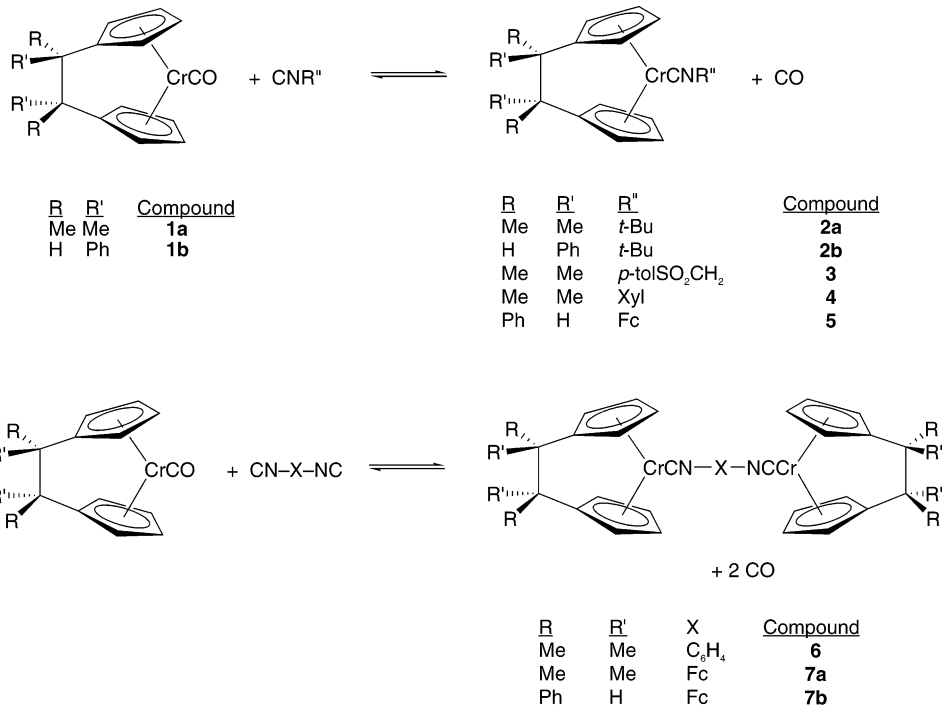

R	R'	Compound
Me	Me	**1a**
H	Ph	**1b**

R	R'	R"	Compound
Me	Me	*t*-Bu	**2a**
H	Ph	*t*-Bu	**2b**
Me	Me	*p*-tolSO$_2$CH$_2$	**3**
Me	Me	Xyl	**4**
Ph	H	Fc	**5**

R	R'	X	Compound
Me	Me	C_6H_4	**6**
Me	Me	Fc	**7a**
Ph	H	Fc	**7b**

This method has enabled us to prepare a series of *ansa*-chromocene isocyanide complexes containing alkyl, aryl, and ferrocenyl isocyanide ligands. With the exception of the ferrocenyl isocyanide derivatives, the redox potentials, molecular structures, isocyanide carbon chemical shifts, and CN stretching frequencies of these complexes exhibit congruous trends that reflect the degree of π-backbonding from the chromium center. One-electron oxidation of the 18*e ansa*-chromocene isocyanide species affords stable, low-spin, 17*e* cations and is accompanied by significant changes in bonding between the chromium and the isocyanide ligand. Density functional theory (DFT) calculations were performed on model complexes in order to elucidate the nature of the bonding between the chromium and the isocyanide ligands and to explain the effects of one-electron oxidation of the complexes.

Results and Discussion

Preparation of *ansa*-Chromocene Isocyanide Complexes. A variety of *ansa*-chromocene isocyanide complexes were prepared according to the reactions shown in Scheme 1. The visible evolution of CO gas indicated the progress of the reaction. Addition of excess isocyanide ligand leads to the formation of unidentified paramagnetic material. As reported previously,[20] the reactions can be reversed by exposing the isocyanide derivatives to an atmosphere of carbon monoxide.

All of the 18*e ansa*-chromocene isocyanide complexes were isolated as air-sensitive, red-brown, microcrystalline solids or powders. The *tert*-butyl isocyanide derivatives, **2a** and **2b**, are both thermally and photochemically sensitive. Over months of storage in a nitrogen atmosphere at room temperature, they form black, shiny paramagnetic materials, the identities of which have not been determined. Both thermolytic and photolytic decomposition of the complexes produces an equivalent of isobutene, presumably from the decomposition of the *tert*-butyl isocyanide ligand. Dealkylation of coordinated isocyanide ligands, particularly *tert*-butyl isocyanide, to form a metal−cyanide linkage has been observed in other complexes.[22−24]

The thermal and photochemical stability of the other isocyanide derivatives was not examined in detail; however, these complexes appear to have a longer shelf life than the *tert*-butyl isocyanide derivatives. Nevertheless, all compounds were stored at −30 °C in the absence of light in order to minimize their decomposition.

X-ray Crystallographic Characterization of *ansa*-Chromocene Isocyanide Complexes. The molecular structures of complexes **2a**, **3**, **4**, **5**, **6**, and **7a** were determined by single-crystal X-ray diffraction. Crystallographic data are listed in Tables 1 and 2. Selected geometrical parameters for the complexes are compared in Tables 3 and 4. The data in Table 3 reveal little variation among the complexes with respect to the geometries of their metallocene fragments. The most distinctive features of the structures are the bonding parameters associated with the isocyanide ligands (compared in Table 4), which reflect the degree of π-backbonding from the chromium to the π^* orbital of the isocyanide ligand. The greater the π-backbonding from the metal, the more carbenoid tautomer **B** contributes to the structure (Figure 1).

The molecular structure of **2a** and its crystal packing diagram are shown in Figure 2. The C17−N1−C18 angle of 131.1(3)° (Table 4) is smaller than the corresponding angle of 139.5(4)° for the related nonbridged molybdocene complex $(C_5H_5)_2$-MoCN-*t*-Bu.[25] The crystal packing diagram for **2a** exhibits a C−H···N interaction between the isocyanide nitrogen of one molecule and a cyclopentadienyl C−H of another. The intermolecular C9−N1 distance of 3.423(4) Å and C9−H9A−N1 angle of 144.2° are characteristic of a weak hydrogen-bonding

(22) Gambarotta, S.; Floriani, C.; Chiesi-Villa, A.; Guastani, C. *Inorg. Chem.* **1984**, *23*, 1739−1747.
(23) Giandomenico, C. M.; Hanau, L. H.; Lippard, S. J. *Organometallics* **1982**, *1*, 142−148.
(24) Dewan, J. C.; Giandomenico, C. M.; Lippard, S. J. *Inorg. Chem.* **1981**, *20*, 4069−4074.
(25) Martins, A. M.; Calhorda, M. J.; Romao, C. C. *J. Organomet. Chem.* **1992**, *423*, 367−390.

Table 1. Crystallographic Data for 2a, [2b][B(C$_6$F$_5$)$_4$], 3, and 4

	2a	**[2b][B(C$_6$F$_5$)$_4$]**	**3**	**4**
formula	$C_{21}H_{29}CrN$	$C_{53}H_{29}BCrF_{20}N$	$C_{25}H_{29}CrNO_2S$	$C_{25}H_{29}CrN$
mol wt	347.45	1122.58	459.55	395.49
cryst syst	monoclinic	triclinic	triclinic	monoclinic
space group	*P*2(1)/*c*	$P\bar{1}$	$P\bar{1}$	*C*2/*c*
a (Å)	9.6236(8)	12.8489(7)	8.2361(6)	10.025(9)
b (Å)	10.3948(9)	13.4768(7)	11.5531(8)	27.72(3)
c (Å)	18.3517(16)	15.3169(8)	12.3836(8)	7.709(7)
α (deg)	90	74.943(1)	75.863(2)	90
β (deg)	93.680(2)	70.386(1)	74.716(2)	112.64(2)
γ (deg)	90	73.237(1)	82.416(2)	90
V (Å^3)	1832.0(3)	2352.9(2)	1099.35(13)	1977(3)
Z	4	2	2	4
T (K)	203(2)	203(2)	203(2)	203(2)
λ (Å)	0.71073	0.71073	0.71073	0.71073
ρ_{calc} (Mg/m^3)	1.260	1.585	1.388	1.329
μ (mm^{-1})	0.624	0.362	0.637	0.588
cryst size (mm^3)	0.14 × 0.09 × 0.06	0.35 × 0.17 × 0.09	0.16 × 0.09 × 0.04	0.27 × 0.07 × 0.03
θ range (deg)	2.12 to 25.25	1.60 to 25.33	1.75 to 28.31	2.32 to 24.99
index ranges	$-11\le h\le 11$, $-12\le k\le 7$, $-22\le l\le 21$	$-15\le h\le 15$, $-16\le k\le 16$, $-18\le l\le 17$	$-10\le h\le 10$, $-15\le k\le 15$, $-15\le l\le 16$	$-11\le h\le 11$, $-32\le k\le 27$, $-9\le l\le 6$
no. reflns collected	10607	22340	11680	8234
no. indep reflns	3316 [*R*(int) = 0.0730]	8594 [*R*(int) = 0.0296]	5439 [*R*(int) = 0.0421]	1739 [*R*(int) = 0.1467]
no. data/restraints/params	3316/0/215	8594/78/675	5439/0/276	1739/0/128
GOF	0.988	1.023	1.085	0.934
R_1 [$I>2\sigma(I)$][a]	0.0498	0.0501	0.0581	0.0621
wR_2 [$I>2\sigma(I)$][b]	0.0938	0.1163	1199	0.1262
largest diff peak, hole (e Å^{-3})	0.323, −0.246	0.718, −0.405	0.458, −0.313	0.441, −0.390

[a] $R_1 = \sum||F_o| - |F_c||/\sum|F_o|$. [b] $wR_2 = \{\sum[w(F_o^2 - F_c^2)^2]/\sum[w(F_o^2)^2]\}^{1/2}$.

Table 2. Crystallographic Data for [4][B(C$_6$F$_5$)$_4$], 5, 6, and 7a

	[4][B(C$_6$F$_5$)$_4$]	**5**	**6**	**7a**
formula	$C_{56}H_{37}BCrF_{20}N$	$C_{35}H_{29}CrFeN$	$C_{40}H_{44}Cr_2N_2$	$C_{50}H_{54}Cr_2FeN_2$
mol wt	1166.68	571.44	656.77	842.80
cryst syst	monoclinic	monoclinic	monoclinic	triclinic
space group	*Cc*	*P*2(1)/*c*	*P*2(1)/*n*	$P\bar{1}$
a (Å)	11.5318(8)	7.641(3)	10.551(9)	12.8945(5)
b (Å)	27.2656(19)	10.176(7)	9.168(8)	13.3213(5)
c (Å)	15.4718(11)	34.17(2	17.063(18)	13.4444(5)
α (deg)	90	90	90	69.17(1)
β (deg)	93.05(2)	95.51(5)	107.79(4)	68.65(1)
γ (deg)	90	90	90	71.84(1)
V (Å^3)	4857.8(6)	2645(3)	1572(3)	1965.8(2)
Z	4	4	2	2
T (K)	203(2)	203(2)	81(2)	81(2)
λ (Å)	0.71073	0.71073	0.71073	0.71073
ρ_{calc} (Mg/m^3)	1.595	1.435	1.388	1.424
μ (mm^{-1})	0.354	0.985	0.724	0.946
cryst size (mm^3)	0.26 × 0.23 × 0.04	0.29 × 0.21 × 0.05	0.23 × 0.08 × 0.03	0.19 × 0.10 × 0.04
θ range (deg)	1.92 to 25.25	2.09 to 27.49	2.03 to 25.47	1.67 to 28.29
index ranges	$-13\le h\le 13$, $-32\le k\le 30$, $-15\le l\le 18$	$-9\le h\le 9$, $-8\le k\le 13$, $-35\le l\le 44$	$-12\le h\le 10$, $-11\le k\le 10$, $-20\le l\le 20$	$-17\le h\le 17$, $-17\le k\le 17$, $-17\le l\le 17$
no. reflns collected	21 193	23 445	10 327	24 182
no. indep reflns	7472 [*R*(int) = 0.0480]	6072 [*R*(int) = 0.0655]	2873 [*R*(int) = 0.1740]	9731 [*R*(int) = 0.0868]
no. data/restraints/params	7472/2/717	6072/0/349	2873/12/199	9731/0/504
GOF	1.014	1.073	0.894	0.967
R_1 [$I>2\sigma(I)$][a]	0.0438	0.0609	0.0640	0.0625
wR_2 [$I>2\sigma(I)$][b]	0.0798	0.1390	0.1251	0.1115
largest diff peak, hole (e Å^{-3})	0.268, −0.251	0.789, −0.494	0.927, −0.773	0.565, −0.523

[a] $R_1 = \sum||F_o| - |F_c||/\sum|F_o|$. [b] $wR_2 = \{\sum[w(F_o^2 - F_c^2)^2]/\sum[w(F_o^2)^2]\}^{1/2}$.

interaction.[26] Similar C−H···N interactions were observed in the X-ray crystal structure of cyanoferrocene, $(C_5H_5)Fe(C_5H_4CN)$, with slightly shorter C- - -N distances of 3.384(6) and 3.381(6) Å.[27] The geometry of the metallocene fragment of **2a** (Table 3) is effectively the same as that of the carbonyl derivative **1a**[19] as shown by the similar angles between the cyclopentadienyl ring planes (**1**, 38.5(5)°; **2a**, 38.7(4)°), the centroid−Cr−centroid angles (**1a**, 143.3(5)°; **2a**, 143.4(2)°), and the average Cr−centroid distances (**1a**, 1.78 Å; **2a**, 1.791 Å).

The molecular structure of **3** and its crystal packing diagram are shown in Figure 3. This complex has an even smaller C17−N−C18 bond angle (123.1(3)°) than **2a** (Table 4). A search of the 2004 Cambridge Data Base showed that only 6 out of 1439 structurally characterized terminal isocyanide-containing transition metal complexes have bending angles in the range 120−130°. The greater *π*-backbonding from the metal in **3** vs **2a** is also manifested in a shortening of the chromium−isocyanide carbon bond distance (Cr−C) and a lengthening of the isocya-

(26) Desiraju, G. R.; Steiner, T. *The Weak Hydrogen Bond*; Oxford University Press: Oxford, 1999.

(27) Bell, W.; Ferguson, G.; Glidewell, C. *Acta Crystallogr.* **1996**, *C52*, 1928−1930.

Table 3. Comparison of Selected Bond Lengths and Angles for Metallocene Portion of Neutral and Cationic *ansa*-Chromocene Isocyanide Complexes[a]

cpd	Cp∠Cp (deg)	Cent[a]−Cr−Cent (deg)	av Cent−Cr (Å)
2a	38.7	143.4	1.792
3	40.1	143.0	1.797
4	38.8	143.1	1.782
5	40.0	143.2	1.802
7	39.1 (Cr1)	143.4	1.792
	39.9 (Cr2)	142.5	1.799
2b$^+$	39.1	141.2	1.821
4$^+$	38.9	141.8	1.818

[a] Cent = ring centroid; Cp∠Cp = dihedral angle between cyclopentadienyl ring planes.

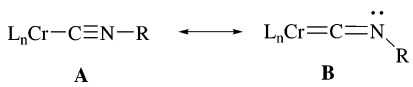

Figure 1. Resonance tautomers of a chromium isocyanide complex.

nide carbon−nitrogen bond (C−N). Three different examples of weak, nonclassical, intermolecular C−H hydrogen bonding are found in the crystal packing diagram of this complex: C12−H12···O1A; C23−H23A···O2B; and C18−H18D···N1C.

Unlike the isocyanide ligands in **2a** and **3**, the terminal xylyl isocyanide ligand in the molecular structure of complex **4** (Figure 4) is perfectly linear because it lies on a crystallographic C_2 axis. The Cr−C9 bond in **4** is longer and the C9−N1 bond is shorter than the corresponding bond lengths in **2a** and **3**, consistent with a lower degree of π-backbonding from the metal. No intermolecular hydrogen-bonding interactions were evident in the crystal packing diagram of this species, consistent with the absence of lone pair electron density on nitrogen and with the reduced accessibility of the nitrogen atom in this crowded molecule. The xylyl moiety is nearly perpendicular to the equatorial wedge of the metallocene, with an 18.4° dihedral angle between the arene ring plane and the centroid−Cr−centroid plane. A similar orientation of the xylyl moiety is seen in the molecular structure of the half-open chromocene complex $Cp(C_5H_7)Cr\{CN\text{-}2,6\text{-}(CH_3)_2C_6H_3\}$;[28] however, in that case the isocyanide is bent with an angle of 166.1(4)°. In the *ansa*-chromocene complex $Me_2Si(C_5Me_4)_2CrCNXyl$, reported by Schaper et al.,[29] the xylyl ring plane is parallel to the equatorial plane of the metallocene, probably due to greater steric interference from the methyl groups on the cyclopentadienyl rings. In this complex, the isocyanide ligand is bent at nitrogen with an angle of 153.2(3)°. The N−C_{aryl} bond distance (1.401(4) Å) in Schaper's complex is significantly longer than that in **4** (1.351(8) Å), which is quite short for a single N−C bond and suggests additional π bonding between the nitrogen and the arene ring. Thus, delocalization of electron density onto the xylyl ring of the isocyanide ligand, as represented by the resonance tautomers in Figure 5, could be partially responsible for the linearity of the isocyanide ligand.

The molecular structure of the isocyanoferrocene derivative **5** is shown in Figure 6. No intermolecular hydrogen-bonding interactions are evident in the crystal packing diagram of **5**. The C25−N1−C26−C30 (4.5(7)°) and C25−N1−C26−C27 (178.1(4)°) torsion angles show that the isocyano-substituted cyclopentadienyl ring of the ferrocene is nearly parallel to the equatorial plane of the chromocene, in contrast to the perpendicular orientation of the xylyl group in **4**. The ferrocenyl C−C bond distances in the isocyano-substituted ring are comparable to each other and to those in the unsubstituted ring. There are relatively few examples of the coordination of isocyanoferrocene to other metals.[30−32] Of these, only the homoleptic $[Cr(CNFc)_6]$ complex of Barybin and co-workers[30] has been structurally characterized. The C25−N1−C27 bond angle in **5** of 134.4(4)° is considerably narrower than the C−N−C(Fc) angles of $[Cr(CNFc)_6]$ (av 162°) and quite similar to the corresponding bond angle in **2a**.

The molecular structure of the homodinuclear complex **6** is shown in Figure 7. The two halves of the molecule are related by a crystallographic inversion center. The phenylene diisocyanide ligand is oriented parallel to the equatorial planes of the *ansa*-chromocene moieties with a dihedral angle of 65.7° between the arene and centroid−Cr−centroid ring planes. Considerable π-backbonding beween the chromium centers and the isocyanide groups is indicated by the small bond angle (128.6°) about the nitrogens and the lengthening of the C−N bonds and shortening of the Cr−C bonds relative to complexes **2a**, **5**, and **4**.

Complexes **7a** and **7b** are rare examples of transition metal complexes containing the diisocyanoferrocene ligand.[33] The only other examples, to our knowledge, are $Fc[(NC)Cr(CO)_5]_2$ and polymeric $[Fc(NC)_2(AuCl)_2]_n$, which were recently reported by Siemeling and co-workers.[10] Repeated efforts to grow crystals of **7b** were unsuccessful. However, **7a** did afford X-ray quality crystals. Figure 8 shows top (a) and side (b) views of the molecular structure of the trinuclear heterometallic complex. The crystal packing diagram in Figure 8c shows the weak C−H···Cr interactions between *ansa*-chromocene fragments of different molecules. The cyclopentadienyl rings of the diisocyanoferrocene are eclipsed, and their rotational conformation places the two *ansa*-chromocene fragments in a *syn* orientation. This arrangement does not appear to be dictated by intra- or intermolecular hydrogen-bonding interactions. Interestingly, a similar conformation was identified for $Fc[(NC)Cr(CO)_5]_2$.[10] The Fc(C)−N−C bond angles for that complex are 174.9° and 170.2°, considerably wider than the corresponding bond angles in **7a** (126.4° and 125.8°).

NMR and IR Spectroscopic Characterization of *ansa*-Chromocene Isocyanide Complexes. Previous studies have shown that there is a correlation between the degree of π-backbonding from the metal to the isocyanide ligand and the C−N stretching frequency, ^{13}C NMR chemical shift, and ^{14}N

Table 4. Comparison of Selected Crystallographic, IR, NMR, and Electrochemical Data for the Cr−CNR Portion of Neutral *ansa*-Chromocene Isocyanide Complexes

cpd	R[a]	Cr−C (Å)	CrC−N (Å)	N−CR (Å)	∠C−N−R (deg)	ν_{C-N} (cm^{-1}) Nujol mull (THF)	$Cr^{II/III}$ (mV) $(E_a+E_c)/2$	^{13}C δ (ppm) C≡NR
2a	*t*-Bu	1.873(3)	1.214(4)	1.482(4)	131.1(3)	1835	−1154	261.2
3	CH_2Tos	1.859(3)	1.226(4)	1.462(4)	123.1(3)	1752 (1774)	−1058	290.6
4	Xyl	1.892(7)	1.195(7)	1.351(8)	180.0(1)	2006 (1980)	−1181	239.6
5	Fc	1.879(4)	1.205(5)	1.411(5)	134.4(4)	1829	−1153	274.0
6	−Ph−	1.861(5)	1.232(6)	1.427(6)	128.6(5)	1766	−1096	278.3
7a	−Fc−	1.862(4)	1.224(4)	1.409(4)	126.4(3)	1751	−1149	278.6
		1.852(4)	1.230(4)	1.415(4)	125.8(3)			

[a] Tos = *p*-tolylsulfonyl; Fc = 1-ferrocenyl; −Fc− = 1,1′-ferrocenyl; −Ph− = 1,4-phenylene.

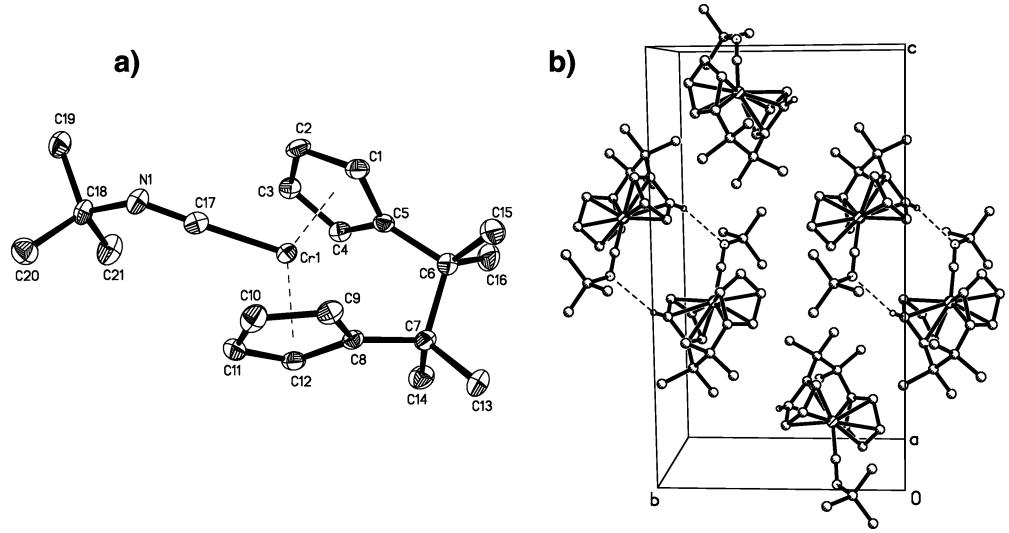

Figure 2. (a) Thermal ellipsoid (30%) drawing of **2a**. Hydrogen atoms are omitted for clarity. (b) Crystal packing diagram illustrating intermolecular hydrogen bonding; C9···N1 3.423(4) Å, C9−H9A···N1 144.2°.

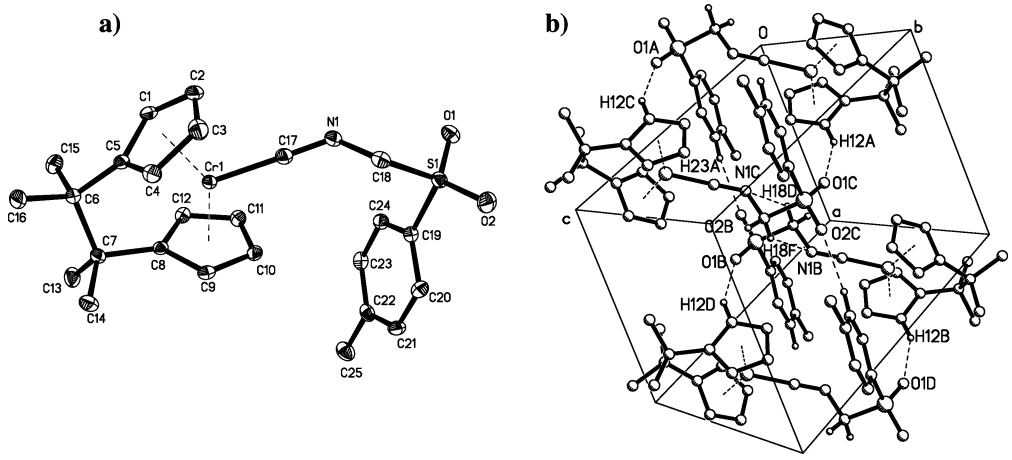

Figure 3. (a) Thermal ellipsoid (30%) drawing of **3**. Hydrogen atoms are omitted for clarity. (b) Crystal packing diagram illustrating weak intermolecular hydrogen bonding. Only hydrogen atoms involved in bonding are shown: C12···O1A 3.267(4) Å, C12−H12···O1A 150.0°; C18···N1B 3.344(4) Å, C18−H18B···N1B 140.7°, C23···O2C 3.314(4) Å, C23−H23···O2C 155.3°.

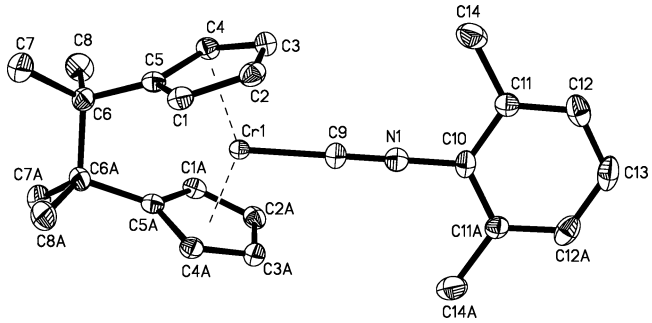

Figure 4. Thermal ellipsoid (30%) drawing of **4**. Hydrogen atoms are omitted for clarity.

NMR chemical shift of the isocyanide ligand.[4,34,35] The IR and ^{13}C NMR spectroscopic data for the neutral 18*e* isocyanide complexes listed in Table 4 roughly exhibit the expected trends. We were not able to detect ^{14}N NMR signals for these complexes, probably due to the low-symmetry environments about the nitrogen atoms.

Since π-backbonding from the metal to the π^* orbital of the isocyanide ligand causes a reduction in the C−N bond order, the magnitude of ν_{C-N} should decrease with increasing π-electron donation from the metal. A plot of C−N stretching frequencies against the crystallographically determined C−N bond lengths (average bond length for **7a**) is shown in Figure 9 (data from Table 4). Deviations from a perfect correlation between the parameters can be attributed at least in part to the fact that the different masses of the substituents on the isocyanide ligands must also influence ν_{C-N}. Furthermore, ν_{C-N} for **3** shifted to 22 cm^{-1} higher energy and ν_{C-N} for **4** shifted to 26 cm^{-1} lower energy when the complexes were analyzed in THF solution instead of a Nujol mull. This shows that the bonding between the metal and the isocyanide ligand is somewhat flexible and is probably influenced by crystal packing forces.

(28) Freeman, J. W.; Hallinan, N. C.; Arif, A. M.; Gedridge, R. W.; Ernst, R. D.; Basolo, F. *J. Am. Chem. Soc.* **1991**, *113*, 6509−6520.
(29) Schaper, F.; Wrobel, O.; Schwoerer, R.; Brintzinger, H.-H. *Organometallics* **2004**, *23*, 3552−3555.
(30) Holovics, T. C.; Deplazes, S. F.; Toriyama, M.; Powell, D. R.; Lushington, G. H.; Barybin, M. V. *Organometallics* **2004**, *23*, 2927−2938.
(31) Knox, G. R.; Pauson, P. L.; Willison, D. *Organometallics* **1990**, *9*, 301−306.
(32) El-Shihi, T.; Siglmueller, F.; Herrmann, R.; Fernanda, M.; Carvalho, N. N.; Pombeiro, A. J. L. *J. Organomet. Chem.* **1987**, *335*, 239−47.
(33) van Leusen, D.; Hessen, B. *Organometallics* **2001**, *20*, 224−226.
(34) Grubisha, D. S.; Rommel, J. S.; Lane, T. M.; Tysoe, W. T.; Bennett, D. W. *Inorg. Chem.* **1992**, *31*, 5022−5027.
(35) Rommel, J. S.; Weinrach, J. B.; Grubisha, D. S.; Bennett, D. W. *Inorg. Chem.* **1988**, *27*, 2945−2949.

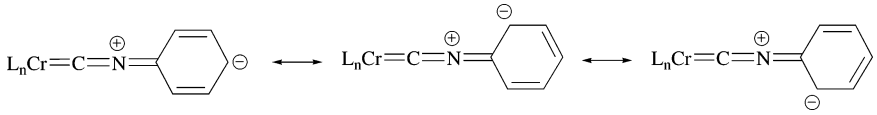

Figure 5. Resonance tautomers that could contribute to the linearity of the isocyanide ligand in **4**.

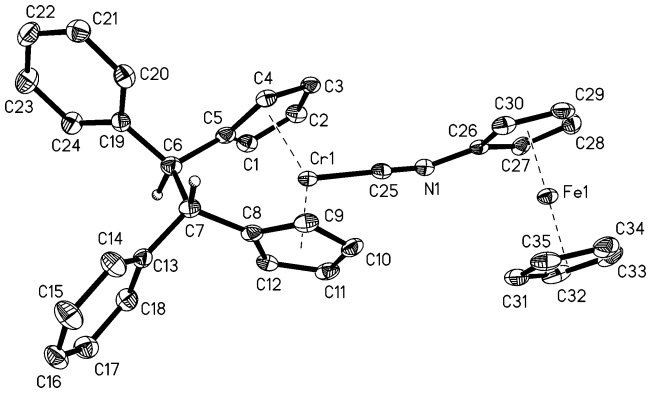

Figure 6. Thermal ellipsoid (30%) drawing of **5**. Only the *ansa* bridge hydrogen atoms are shown for clarity. Selected bond lengths (Å) and angles (deg): C26−C27 1.411(5), C26−C30 1.436(6), C27−C28 1.422(6), C29−C30 1.412(6), C29−C28 1.399(6), C31−C32 1.393(7), C31−C35 1.420(0), C32−C33 1.404(7), C33−C34 1.403(7), C34−C35 1.409(7), C25−N1−C26 134.4(4), C25−N1−C26−C30 4.5(7), C25−N1−C26−C27 178.1(4).

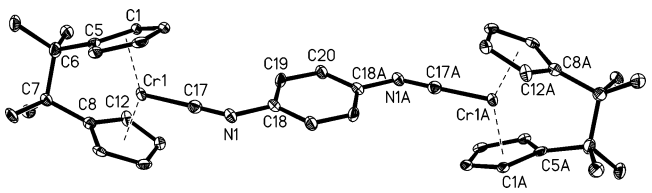

Figure 7. Thermal ellipsoid (30%) drawing of **6**. Hydrogen atoms are omitted for clarity. Selected bond lengths (Å): C18−C19 1.386(7), C19−C20 1.395(6), C20−C18A 1.399(7).

The trend in ^{13}C chemical shifts for the complexes is consistent with that observed for other transition metal isocyanide complexes. The isocyanide carbon resonance shifts *downfield* with increasing M−C π bonding because the M−C π bonding increases the magnitude of the negative-valued paramagnetic shielding constant (σ_p). This constant dominates the chemical shift for atoms, such as carbon, with 2pπ electrons.[4,34,35] Plots of redox potential (Figure 10a) and ν_{C-N} (Figure 10b) against ^{13}C chemical shift show the expected general trends; the ^{13}C chemical shifts increase with increasing redox potential and decreasing ν_{C-N}.

Electrochemical Measurements. The isocyanide complexes exhibit a quasi-reversible $Cr^{II/III}$ couple and an anodic peak at higher potential for the oxidation of Cr^{III} to Cr^{IV}, the electrochemical irreversibility of which has been attributed to the coordination of the THF solvent by Cr^{IV}.[36] The $Cr^{II/III}$ redox potentials for the complexes (referenced to $(C_5H_5)_2Fe^{0/1+}$) are listed in Table 4. With the exception of **7a**, there is good correlation between the redox potentials of the complexes and the π-accepting character of the isocyanide ligands. In general, the redox potentials of the complexes increase with increasing M−C π-backbonding (as reflected in the structural and spectroscopic parameters). This behavior has been observed in a variety of other metal isocyanide complexes, and the redox potential of the metal complex has even been used to parametrize the electron donor/acceptor character of the isocyanide ligand.[37]

Interestingly, the $Cr^{II/III}$ potential for **2a** is similar to that of **5**. This indicates that the electronic effect of a ferrocenyl moiety is comparable to that of a *tert*-butyl group in the *ansa*-chromocene system. The similar ν(CN) and ∠C−N−R values for **2b** and **5** (Table 4) also support this conclusion. This contrasts with the findings for $Cr(CNR)_6$ and $(CO)_5CrCNR$ complexes, in which the ferrocenyl moiety behaves more like an aryl group than an alkyl group.[1,10,30]

Cyclic voltammograms of complexes **6** and **7a** are shown in Figure 11. The appearance of only one $Cr^{II/III}$ redox couple for these complexes indicates that there is little if any electronic communication between the chromium centers via the diisocyanoferrocene and phenylene diisocyanide bridges. The cyclic voltammogram for **7b** is similar to that of **7a**. Each of the voltammograms exhibits an electrochemically irreversible $Cr^{III/IV}$ couple. The redox potentials of the coordinated isocyano- and diisocyanoferrocene ligands in **5**, **7a**, and **7b** are more positive than even the anodic wave for the oxidation of Cr^{III} to Cr^{IV}. The iron-centered redox potential in **5** (282 mV) is almost 100 mV higher than that of the free isocyanoferrocene ligand (186 mV). It can be argued that this positive shift in the redox potential is due to the electron-withdrawing properties of Cr^{IV}. On the other hand, the iron-centered redox potential in **7a** (589 mV) is 50 mV lower than that of free diisocyanoferrocene (639 mV). It is possible that the diisocyanoferrocene ligand is dissociated from the *ansa*-chromocene dications at this point, since there is evidence of free isocyanoferrocene in the IR spectrum of **[7b][PF$_6$]$_2$**, in which the *ansa*-chromocenes are only monocations. Efforts to attach only one *ansa*-chromocene moiety to diisocyanoferrocene for comparison were unsuccessful. The 1:1 reaction between **1a** and diisocyanoferrocene afforded only **7a** and half an equivalent of unreacted diisocyanoferrocene.[38]

Chemical Oxidation of the *ansa*-Chromocene Complexes. One-electron oxidation of the isocyanide complexes was accomplished using either trityl or ferrocenium salts to form low-spin, 17*e* cations that are red-brown in color, like the neutral, 18*e* species (Scheme 2). Magnetic susceptibility measurements on the monocations gave spin-only magnetic moments consistent with one unpaired electron on the metal: **[2b][B(C$_6$F$_5$)$_4$]** (μ_{eff} = 1.8 μ_B), **[4][B(C$_6$F$_5$)$_4$]** (μ_{eff} = 1.9 μ_B), **[5]PF$_6$** (μ_{eff} = 1.9 μ_B). Since selective oxidation of only one *ansa*-chromocene moiety in the diisocyanide-bridged complexes was not feasible, both were oxidized to form the dications **[6][B(Ar$_F$)$_4$]$_2$** (μ_{eff} = 2.3 μ_B; Ar$_F$ = 3,5-(CF$_3$)$_2$C$_6$H$_3$) and **[7b][PF$_6$]$_2$** (μ_{eff} = 2.6 μ_B). The magnetic moments of these polynuclear complexes correspond to magnetic moments of 1.6 μ_B (**7b^{2+}**) and 1.8 μ_B (**6^{2+}**) per chromium center.[39] This supports our conclusion from the cyclic voltammetry that there is no electronic interaction between chromium centers via the phenylene or ferrocenylene bridge.

X-ray quality crystals of **[2b][B(C$_6$F$_5$)$_4$]** and **[4][B(C$_6$F$_5$)$_4$]** were obtained for molecular structure determinations. Their

(36) van Raaij, E. U.; Brintzinger, H. H. *J. Organomet. Chem.* **1988**, *356*, 315−323.

(37) Pombeiro, A. J. L. *Inorg. Chim. Acta* **1985**, *103*, 95−103.

(38) A reviewer suggested that the selectivity for the heterotrinuclear species over the heterodinuclear species in the 1:1 reaction between **1a** and diisocyanoferrocene may be entropic in nature since the first coordinated *ansa*-chromocene should impede the rotation of the noncoordinated ferrocene ring, facilitating the coordination of a second *ansa*-chromocene fragment.

(39) Since μ_{eff} is proportional to $\sqrt{\chi_M}$, μ_{eff} for each *ansa*-chromocene moiety was estimated by dividing χ_M for the entire molecule by $\sqrt{2}$.

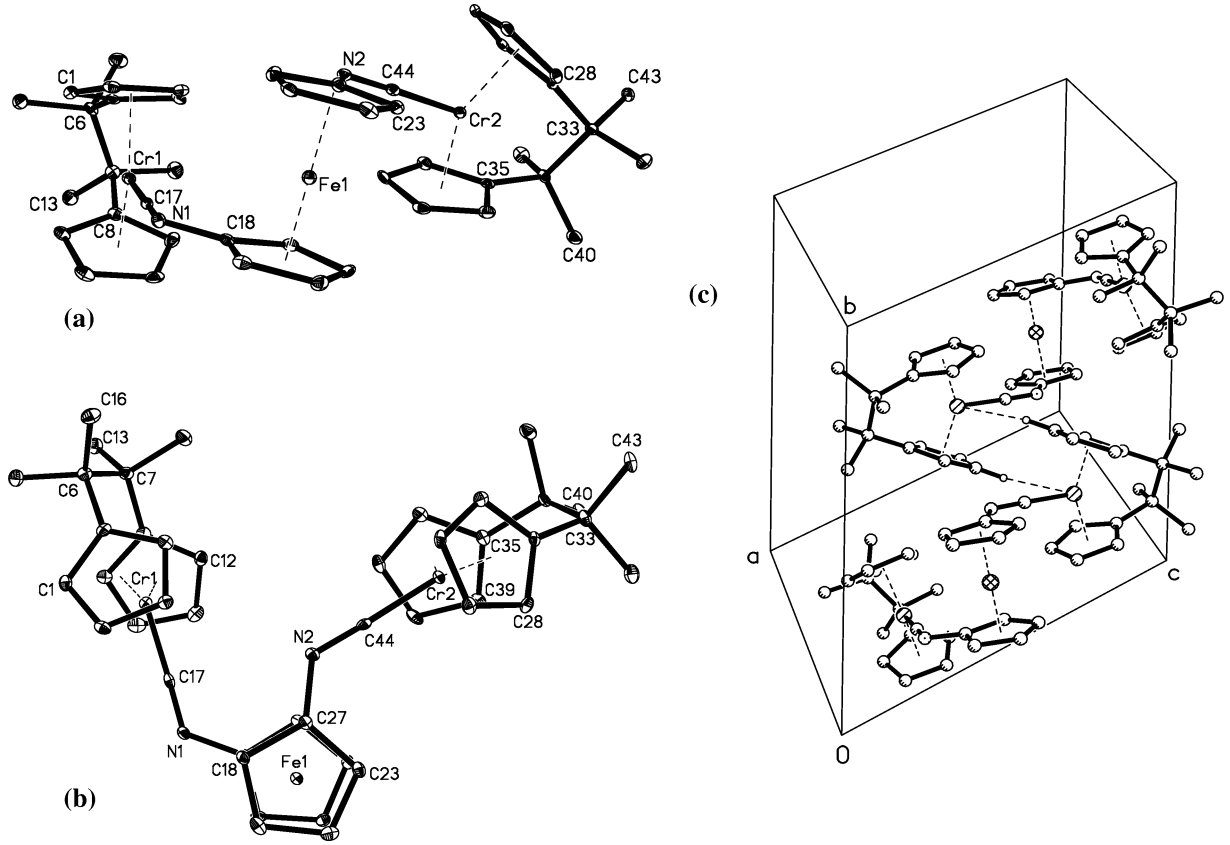

Figure 8. Thermal ellipsoid (30%) drawing of **7a**: (a) side view, (b) top view, and (c) crystal packing diagram illustrating intermolecular hydrogen bonding. Only the hydrogen atoms involved in bonding are shown.

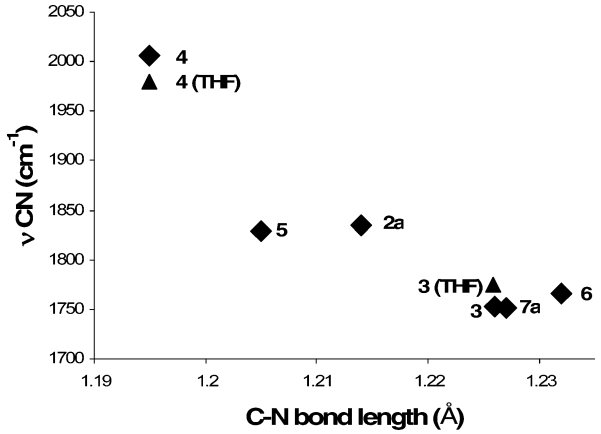

Figure 9. Plot of C−N stretching frequencies (measured in Nujol mull unless otherwise indicated) vs Cr−N bond length (an average between the two C−N bond distances of **7a** was used).

crystallographic data are listed in Table 1. Thermal ellipsoid drawings of the cations $\mathbf{2b}^+$ and $\mathbf{4}^+$ are shown in Figures 12 and 13, respectively, along with selected bond lengths and angles.

Removal of an electron from **2b** results in a straightening of the *tert*-butyl isocyanide ligand, which is close to linear in **[2b][B(C$_6$F$_5$)$_4$]**, with a C13−N1−C14 bond angle of 173.9(4)°. The Cr−C13 bond is significantly longer and the C13−N1 bond is significantly shorter than the corresponding bond lengths in **2b**. All of this is a reflection of the poorer π-backbonding ability of the cationic chromium center. Two IR bands at 2199 and 2139 cm^{-1} (Nujol mull) were observed for this complex. Neither band corresponds to the neutral complex, **2b**. We attribute the second band to free *t*-BuNC (ν NC = 2140 cm^{-1}). The 2199 cm^{-1} band is higher in energy than that of the free isocyanide and only slightly lower than that of [Cp$_3$ZrCN-*t*-Bu]$^+$ (2209 cm^{-1}),[40] indicating that the interaction between the isocyanide ligand and chromium is primarily σ in nature.

Since the xylyl isocyanide ligand does not lie on an axis of symmetry in **[4][B(C$_6$F$_5$)$_4$]**, as it does in **4**, it is not perfectly linear but nearly so. The Cr−C17 bond is longer and the C17−N1 bond is shorter than the corresponding bonds in the neutral complex, due to reduced π-backbonding from the metal. The N−C(aryl) bond distance (N1−C18, 1.396(5) Å) is longer than that in **4** (1.351(8) Å), indicating less π e^- delocalization from the Cr to the arene ring. The orientation of the xylyl moiety is nearly perpendicular to the equatorial wedge, similar to the neutral complex, with a 19.3° dihedral angle between the arene ring plane and the centroid−Cr−centroid plane. The energy of the C−N stretch for this compound is 2119 cm^{-1}, which is comparable to that of the free ligand (2115 cm^{-1}).

We were unable to obtain X-ray quality crystals of either **[5][PF$_6$]** and **[7b][PF$_6$]$_2$**. The energy of the C−N stretch for **[5][PF$_6$]** of 2118 cm^{-1} is similar to that of the free isocyanide (ν = 2121 cm^{-1}). Two C−N stretches were observed for **[7b][PF$_6$]$_2$** at 2113 and 2137 cm^{-1}. We attribute the lower energy band to free diisocyanoferrocene (ν = 2114 cm^{-1}) and the higher energy band to the dication.

An X-ray crystal structure determination for **[6][B(Ar$_F$)$_4$]$_2$** was performed, but the quality of the crystal was so poor that we could not refine the structure beyond an *R* value of 12.5%. A preliminary thermal ellipsoid drawing of the dication is shown in Figure 14. The phenylene diisocyanide bridge is clearly linear in **[6][B(Ar$_F$)$_4$]$_2$**, in contrast to its zigzag geometry in the neutral complex. The C−N stretch for this complex occurs at 2088

(40) Brackemeyer, T.; Erker, G.; Fröhlich, R. *Organometallics* **1997**, *16*, 531−536.

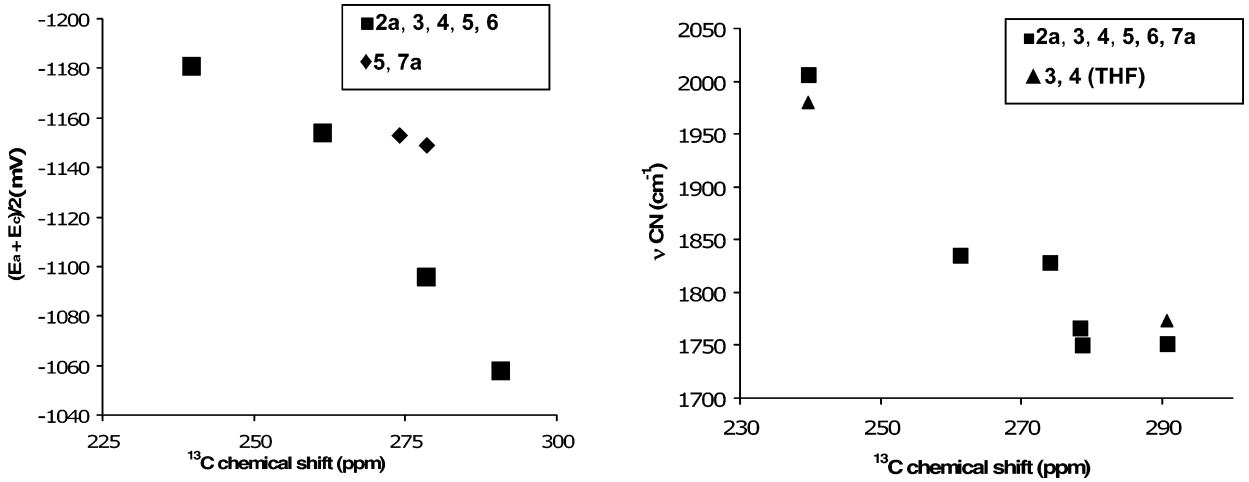

Figure 10. Plot of (left) redox potential vs isocyanide ^{13}C chemical shift and (right) $\nu C{-}N$ vs isocyanide ^{13}C chemical shift for the *ansa*-chromocene isocyanide complexes.

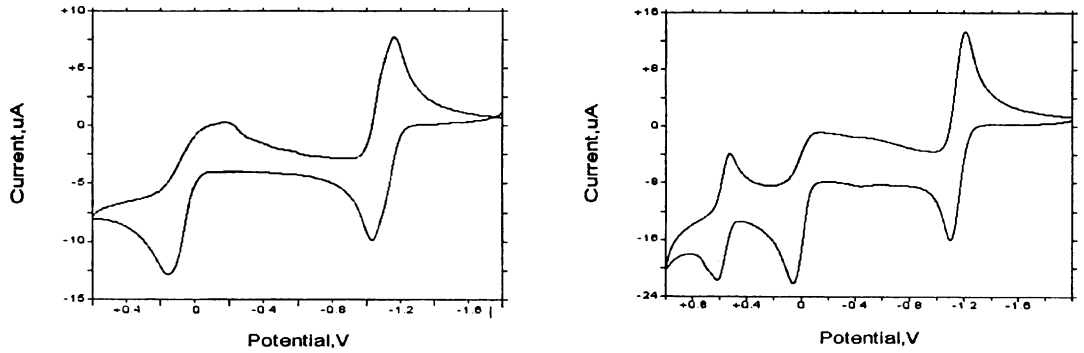

Figure 11. Cyclic voltammograms of complexes **6** (left) and **7a** (right) (scan rate 25 mV/s).

Scheme 2

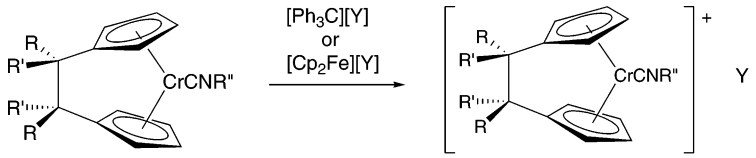

R	R'	R"	Y⁻	Cation
H	Ph	*t*-Bu	$B(C_6F_5)_4$	**2b**$^+$
Me	Me	xyl	$B(C_6F_5)_4$	**4**$^+$
Ph	H	Fc	PF_6	**5**$^+$

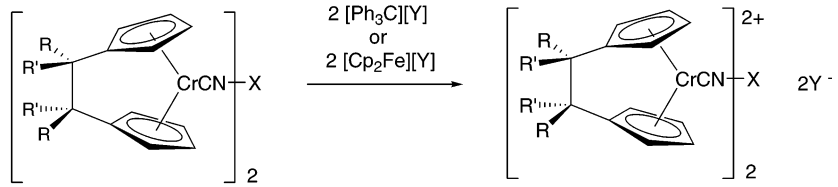

R	R'	X	Y	Cation
Me	Me	C_6H_4	$B(C_6F_5)_4$	**6**$^{2+}$
Ph	H	Fc	PF_6	**7b**$^{2+}$

cm^{-1}, somewhat lower in energy than that of the free phenylene diisocyanide ligand ($\nu = 2118$ cm^{-1}) but substantially higher than that of **6** (1766 cm^{-1}).

The bonding between the chromium and its cyclopentadienyl rings appears to be unaffected by one-electron oxidation of the metal since the structural parameters of the metallocene fragments of the cations are similar to those of the neutral complexes (Table 3). Thus, the change in the oxidation state of the metal is mostly manifested in its interaction with the isocyanide ligand.

Calculations. The structures of models for complexes **2**−**6** (containing a CH_2CH_2 bridge instead of the CMe_2CMe_2 and CHPhCHPh bridges used experimentally) were studied using DFT methods. Geometries of all neutral 18*e* and cationic 17*e* species were fully optimized at the RIBP86/SV(P) level, and

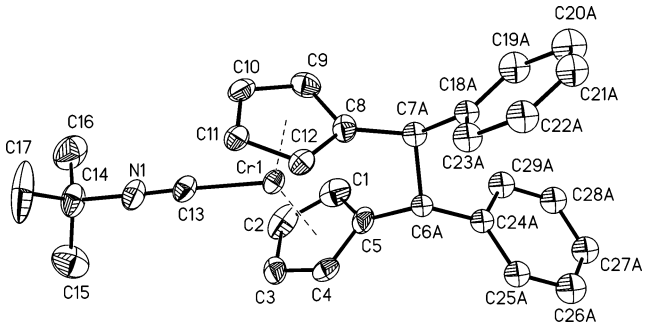

Figure 12. Thermal ellipsoid (30%) drawing of **[2b][B(C$_6$F$_5$)$_4$]**. Only the cation is shown. Hydrogen atoms are omitted for clarity. Selected bond lengths (Å) and angles (deg): Cr1−C13 1.956(3), C13−N1 1.155(4), av Cr−centroid 1.821, C13−N1−C14 173.9(4). Only part of the disordered *ansa*-bridge is displayed.

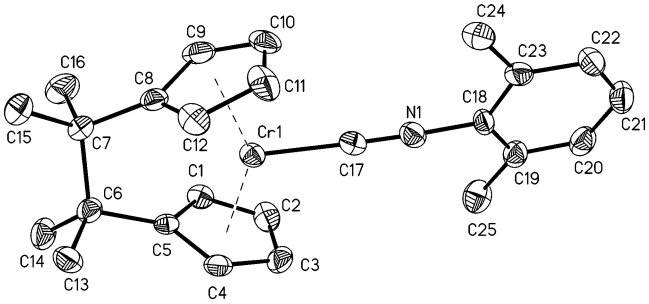

Figure 13. Thermal ellipsoid (30%) drawing of **[4][B(C$_6$F$_5$)$_4$]**. Only the cation is shown. Hydrogen atoms are omitted for clarity. Selected bond lengths (Å) and angles (deg): Cr1−C17 1.933(5), C17−N1 1.174(5), N1−C18 1.396(5), C18−C19 1.404(6), C18−C23 1.390(6), C19−C20 1.378(6), C20−C21 1.378(7), C21−C22 1.383(8), C22−C23 (1.393(6), C17−N1−C18 178.8(4).

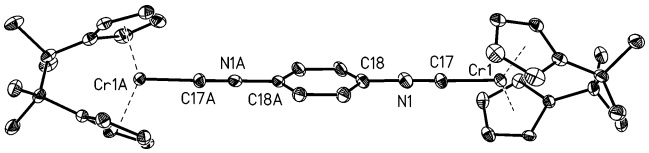

Figure 14. Preliminary thermal ellipsoid (30%) drawing of **[6]-[B(Ar$_F$)$_4$]$_2$**. Only the dication is shown.

improved energies were obtained from single-point b3-lyp/TZVP calculations including a COSMO solvation correction ($\epsilon = 7.5$); this correction is particularly important for the cationic species. The resulting geometric parameters are collected and compared with experimental values in Table 5; energy-derived data are listed in Table 6.

i. Geometries. One of the advantages of using calculated structures is the lack of "random" variations found in X-ray structures due to packing effects and noise. Systematic errors can still be important, but trends often appear more clearly from calculated data. For the neutral complexes, for which we have collected a fair amount of structural data, the calculated Cr−$C_{isocyanide}$ distance is typically too short by 0.01−0.02 Å, while the calculated C═N bond is usually too long by roughly the same amount (this bond length is also overestimated for the free ligands). The spread in both parameters induced by ligand variation is larger than this, and the experimental and calculated data both show the inverse correlation between the two bond lengths, as can be seen in the plot of both experimental and calculated Cr−$C_{isocyanide}$ bond lengths vs C═N bond lengths for the neutral complexes in Figure 15a. For the cationic complexes, only three X-ray structures are available, one of which is of insufficient quality to trust the bond lengths. Here, use of the calculated data is revealing. In contrast to the neutral complexes, the cations show virtually no changes in the C═N bond length, even though the Cr−C bond length changes appreciably (Figure 15b). The difference between neutral and cationic species must be due to a difference in bonding interaction. In the neutral complexes, π-backbonding dominates. Small, electron-withdrawing substituents on the ligand (e.g. CH_2Tos) increase π-backbonding and, hence, produce shorter Cr−C and longer C═N bonds. For the cation, π-backbonding appears to be relatively unimportant, and the isocyanide functions mainly as a σ-donor. The C═N bond lengths are nearly identical to those calculated for the free ligands, and the Cr−C bond length appears to be determined mainly by the steric bulk of the substituent at nitrogen, *t*-Bu and Xyl giving the largest distances.

We have calculated the structures of both "parallel" and "perpendicular" conformations of the PhNC and XylNC complexes. These conformations are very similar in energy for the neutral as well as the cationic complexes. However, the C═N bond lengths are significantly different *for the neutral complexes only*. On going from the planar to the perpendicular conformation, the C−N−C angle opens up (by ca. 20°), the Cr−C bond becomes longer, and the C═N distance becomes smaller, all of which indicates decreased π-backbonding. The fact that this is not accompanied by a large change in energy demonstrates that the bonding situation in these molecules is rather fluid and can easily adapt itself to electronic or steric variations of the ligand.

The calculated monocation of the phenylene-bridged dinuclear system shows clearly localized Cr^{II} and Cr^{III} centers characterized by very different C−N−C angles.

ii. Electronic Structures of the Cations. The highest occupied orbitals of the cationic complexes are not well-separated, making it difficult to interpret the nature of the oxidized state. However, the orbital plot of the β LUMO (shown in Figure 16 for the analogue of $\mathbf{5}^+$) clearly shows that oxidation has removed an electron from a d_{z^2}-like orbital lying in the wedge between the two Cp rings, perpendicular to the Cr−N bond. This orbital is similar to the highest occupied molecular orbital of Cp_2CrCO determined by Lauher and Hoffman in 1976 using extended Hückel theory[41] and more recently by Green et al. using density functional theory.[18] The spin-density plot (not shown) shows that there is a small amount of spin polarization on the Cr-bound Cp rings, but virtually no spin density on the ferrocenyl group. This is because the oxidation occurs essentially in the σ system, so the effects are not communicated efficiently via the cyclopentadienyl π system of the ferrocenyl moiety. Presumably, this is also part of the reason we see virtually no communication between the oxidized centers in the bridged dinuclear systems. The nonbonding nature of this orbital explains why removal of an electron from it does not result in large geometrical changes in the chromocene fragment. This orbital cannot have been involved directly in Cr−isocyanide π-backbonding, because it is of the wrong symmetry. However, removing an electron from it lowers the levels of all remaining occupied chromium d orbitals and so makes them less available for electron back-donation.

iii. Energies. To facilitate interpretation of the results, we have included the CO complex as a reference compound. Table 6 shows relative binding energies of CO and isocyanides to the *ansa*-chromocene fragment. Apparently, *all* isocyanides bind somewhat more weakly than CO. This is not very surprising: in the neutral systems, π-backbonding dominates, and this will be stronger for CO than for any isocyanide ligand. Of the

(41) Lauher, J. W.; Hoffman, R. *J. Am. Chem. Soc.* **1976**, *98*, 1729−1741.

Table 5. Geometrical Parameters (Å, deg) for Calculated and Observed Structures

		free ligand		complex				C═N
ligand		C−N	N−C	Cr−C	C−N	N−C	∠CNC	elongation
				Neutral Complexes				
CO	calc	(1.142)		1.855	(1.174)			0.032
CNH	calc	1.185		1.851	1.232		122.0	0.047
CN*t*Bu	X-ray	1.145[b]	1.469	1.873(3)	1.214(4)	1.482(4)	131.1(3)	0.069
	calc	1.188	1.444	1.869	1.223	1.474	136.5	0.035
CNTs	X-ray	1.155[c]	1.430	1.859(3)	1.226(4)	1.462(4)	123.1(3)	0.048
	calc	1.190	1.399	1.842	1.238	1.423	130.5	0.048
CNPh	calc	1.191	1.385	1.875	1.211	1.366	166.2	0.020
	calc (par)			1.849	1.232	1.402	136.1	
CNXyl	X-ray	1.160[d]	1.400	1.892(7)	1.195(7)	1.351(8)	180	0.035
	calc	1.192	1.386	1.880	1.213	1.373	163.4	0.021
	calc (par)			1.869	1.224	1.392	148.8	0.032
CNFc	X-ray	1.157[e]	1.389	1.879(4)	1.205(5)	1.411(5)	134.4(4)	0.048
	calc	1.191	1.375	1.852	1.231	1.393	135.0	0.040
CNPhNC	X-ray	1.163[f]	1.393	1.861(5)	1.232(6)	1.427(6)	128.6(5)	0.069
	calc (C_2H_4)	1.192	1.382	1.849	1.233	1.401	134.6	0.041
	calc (C_2Me_4)			1.843	1.234	1.402	132.2	0.042
CNPhNC	calc (C_2H_4)			1.848	1.227	1.395	138.1	
(monocation)	calc (C_2Me_4)			1.841	1.229	1.397	134.6	
CNFcNC	X-ray			1.852(4)	1.230(4)	1.415(4)	125.8(3)	
				1.862(4)	1.224(4)		126.4(3)	
				Cations				
CO	calc	(1.142)		1.867	(1.159)			0.017
CNH	calc	1.185		1.886	1.198		147.5	0.013
CN*t*Bu	X-ray	1.145[b]	1.469	1.956(3)	1.155(4)	1.455(4)	173.9(4)	0.014
	calc	1.188	1.444	1.931	1.186	1.450	178.7	−0.002
CNTs	calc	1.190	1.399	1.891	1.197	1.401	158.8	0.007
CNPh	calc	1.191	1.385	1.915	1.191	1.381	177.1	0.000
	calc (par)			1.914	1.192	1.384	178.2	
CNXyl	X-ray			1.933(5)	1.174(5)	1.396(5)	178.8(4)	0.014
	calc	1.192	1.386	1.927	1.192	1.382	179.4	0.000
	calc (par)			1.919	1.192	1.384	176.9	0.000
CNFc	calc	1.191	1.375	1.918	1.192	1.371	173.2	0.001
CNC_6H_4NC	calc (C_2H_4)	1.192	1.382	1.888	1.201	1.376	176.9	0.009
(monocation)	calc (C_2Me_4)			1.882	1.200	1.373	179.5	0.008
CNC_6H_4NC	X-ray[a]	1.163[e]	1.393	1.942(8)	1.156(10)	1.411(10)	177.9(9)	−0.007
	calc (C_2H_4)	1.192	1.382	1.899	1.197	1.376	179.3	0.005
	calc (C_2Me_4)			1.896	1.199	1.375	179.5	0.007

[a] Poor quality structure. [b] Tada, H.; Tozyo, T.; Shiro, M. *J. Org. Chem.* **1988**, *53*, 3366 (for a *t*-alkylNC). [c] Weener, J.-W.; Versleijen, J. P. G.; Meetsma, A.; ten Hoeve, W.; van Leusen, A. M. *Eur. J. Org. Chem.* **1998**, *1511*, 1 (for a $CNCH_2$-phosphonate). [d] Mathieson, T.; Schier, A.; Schmidbaur, H. *J. Chem. Soc., Dalton Trans.* **2001**, 1196. [e] Wrackmeyer, B.; Maisel, H. E.; Tok, O. L.; Milius,W.; Herberhold, M. *Z. Anorg. Allg. Chem.* **2004**, *630*, 2106−2109. [f] Colapietro, M.; Domenicano, A.; Portalone, G.; Torrini, I.; Hargittai, I.; Schultz, G. *J. Mol. Struct.* **1984**, *125*, 19.

Table 6. Calculated Complexation Energies and Oxidation Potentials

	E_{compl} (kcal/mol)[a]		E_{ox} (mV)[b]	
ligand	neutral	cation	calc	obs
CO	(0)	(0)	−880	
CNH	3.54	−1.66	−1106	
CN*t*Bu	10.21	−2.07	−1413	−1154
CNPh	3.96	−3.75	−1215	
CNXyl	6.85	−2.11	−1269	−1181
CNFc	5.23	−2.32	−1208	−1153
CNTs	0.62	−3.47	(−1058)	−1058
CNC_6H_4NC	2.91		−1128	−1096

[a] Relative to the CO complexes. [b] For calculated data, E_{ox} for CNTs arbitrarily fixed at its experimental value.

isocyanide complexes studied, the tosyl-substituted derivative is the best π-acceptor and binds most strongly.

In the cationic complexes, all ligands bind more strongly than CO, but the differences between ligands are very small, consistent with the interpretation that σ-donation dominates and is relatively insensitive to electronic effects. The correlation between calculated and experimental redox potentials (Figure 17) is fair, *except* for the *t*-BuNC derivative, for which the calculated value is much too negative. At present we do not have an explanation for this discrepancy.

Summary and Conclusions

Ligand substitution on *ansa*-chromocene carbonyl precursors is a general route to a variety of *ansa*-chromocene isocyanide derivatives. We have yet to determine the mechanism for this ligand substitution reaction; however, we suspect that the substitution of CO by isocyanide ligands is associative in nature for the following reasons: (a) Brintzinger and co-workers have identified *ansa*-chromocene dicarbonyl complexes,[36,42] showing that ring slippage can occur to accommodate a second 2*e*-donating ligand on the metal. Furthermore, this ring slippage is catalyzed by small amounts of oxidants, indicating that one-electron oxidation of the *ansa*-chromocene carbonyl complex facilitates ring slippage;[36] (b) it is difficult to remove CO from the neutral and cationic complexes by either thermal or photochemical means.[43]

There is fairly good agreement among the crystallographic, IR, NMR, and electrochemical data with respect to the π-acceptor strength of the isocyanide ligands, giving the ordering $CNCH_2Tos$ > FcNC ≈ *t*-BuNC > CNXyl.

Consistent with the experimental data, DFT calculations indicate that CrCNR bonding in the neutral complexes is dominated by π-back-donation. The amount of backbonding is

(42) Schaper, F.; Rentzsch, M.; Prosec, M.-H.; Rief, U.; Schmidt, K.; Brintzinger, H. H. *J. Organomet. Chem.* **1997**, *534*, 67−69.

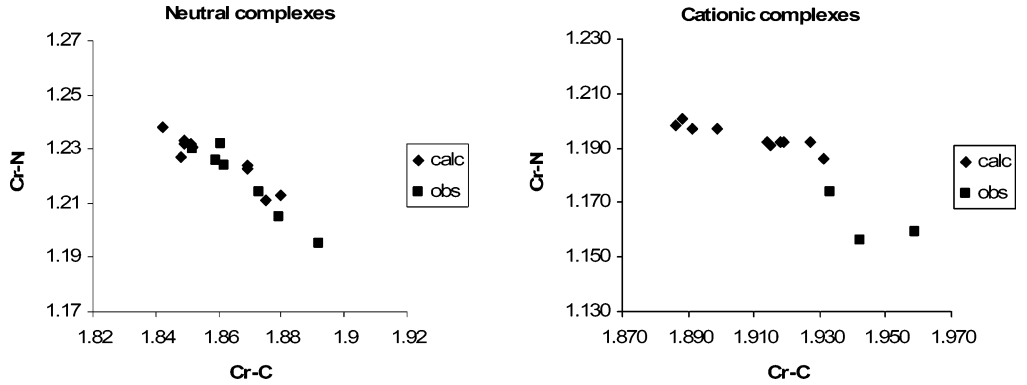

Figure 15. C−N vs Cr−C bond lengths (Å) for all calculated and observed neutral (left) and cationic (right) structures.

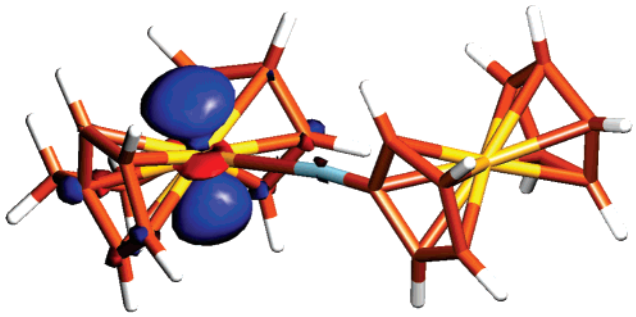

Figure 16. β-LUMO for model of cation $\mathbf{5}^{+}$.

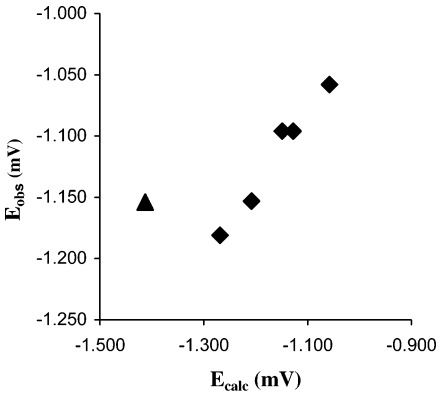

Figure 17. Calculated vs observed oxidation potentials (triangular data point is for *t*-Bu isocyanide derivative).

sensitive to the steric and electronic properties of the ligands, but changes in backbonding are associated with relatively small energy changes. In the 17*e* cationic species, back-donation is greatly diminished, and σ-donation is the dominant interaction.

Since oxidation occurs from a chromocene orbital that does not interact with any π orbital on the isocyanide ligand, there is little communication between the oxidized Cr center and any π system attached to the isocyano group. This provides a rationale for the lack of communication between the metal centers in the phenylene- and ferrocenylene-bridged systems.

Experimental Section

General Procedures. All manipulations were performed under dinitrogen, argon, or vacuum using a combination of glovebox, high-vacuum, and Schlenk techniques. HPLC grade solvents were dried by passage over alumina and then stored in line pots from which they were vacuum transferred from sodium/benzophenone. Argon was purified by passage over an oxy tower BASF catalyst (Aldrich) and 4A molecular sieves. Deuterated solvents were dried over 4A molecular sieves and stored in the glovebox. HPLC grade tetrahydrofuran (Fisher) was used as received for electrochemical measurements.

NMR spectra were recorded on Bruker Avance 300MB (300 MHz ^{1}H; 75.4 MHz, ^{13}C; 78 MHz, ^{27}Al) and a Bruker Avance 500 (500 MHz ^{1}H; 125 MHz ^{13}C; 470 MHz ^{19}F; 202 MHz ^{31}P) spectrometers. ^{1}H and ^{13}C chemical shifts were referenced to solvent, and ^{19}F and ^{13}P chemical shifts were referenced to external standards ($BF_3(OEt_2)$, δ 0; H_3PO_4(80% aq), δ 0).

Cyclic voltammetry measurements were performed on a BAS CV50W voltammetric analyzer in a nitrogen-filled glovebox. Potentials were measured, without IR compensation, against a reference electrode consisting of a silver wire immersed in a solution of $AgNO_3$ (0.01 M) in acetonitrile, using a glassy carbon working electrode and a platinum wire as the counter electrode. Measurements were performed on THF solutions of the sample complex (<1 mM) containing 0.3 M $[NBu_4][PF_6]$ electrolyte. All potentials are referenced to the ferrocene$^{0/1+}$ couple ($E_p \approx 200$ mV), which was measured separately prior to each sample measurement.

IR spectra were obtained on an ATI Mattson Genesis Series FTIR spectrophotometer and on a Bio Rad FT-IR spectrometer FTS 175C. NIR spectra were obtained on a Perkin-Elmer 330 spectrophotometer. The samples were measured as THF solutions of the complexes under nitrogen in sealed 1 cm quartz cuvettes.

Magnetic susceptibilities were determined on either solid samples of the complexes using a Johnson Matthey magnetic susceptibility balance type MSB, model MK I, or on solution samples according to the Evans NMR method.[44] Molar magnetic susceptibilities were corrected for diamagnetism using Pascal constants.[45]

Elemental analyses were determined by Desert Analytics (Tuscon, AZ). In some cases the carbon values were 1−3% below theoretical. In one case (compound **7b**) addition of WO_3 to the sample prior to combustion improved the carbon value. Therefore, the low carbon values could be partly due to incomplete combustion. With the exception of paramagnetic **[7b][PF$_6$]$_2$**, ^{1}H NMR spectra have been deposited in the Supporting Information for compounds whose analyses were out of range.

Complexes **1a**, **1b**, **2a**, and **2b** were prepared as described previously.[20,21] Isocyanoferrocene was prepared in six steps starting from ferrocene according to literature preparations. Aminoferrocene was prepared as described by Bildstein et al.[46] This was converted to isocyanoferrocene in a slightly modified version of the synthesis described by Knox et al.[31] A more efficient method for preparing isocyanoferrocene from aminoferrocene was recently reported by Holovics et al.[30] Diisocyanoferrocene was prepared as described

(43) Perrotin, P.; Shapiro, P. J., unreported results.
(44) Evans, D. F. *J. Am. Chem. Soc.* **1959**, *92*, 2003−2005.
(45) König, E.; König, G. K. *Magnetic Properties of Coordination and Organometallic Transition Metal Compounds*; Hellwege, K.-H., Hellweg, A. M., Eds.; Springer-Verlag: Berlin, 1981; Vol. 11.
(46) Bildstein, B.; Malaun, M.; Kopacka, H.; Wurst, K.; Mitterboeck, M.; Ongania, K. H.; Opromeolla, G.; Zanello, P. *Organometallics* **1999**, *18*, 4325−4336.

by van Leusen and Hessen.[33] $[(C_5H_5)_2Fe][B(Ar_F)_4]$ (Ar_F = 3,5-$(CF_3)C_6H_3$) was prepared according to a literature procedure[47] and recrystallized from CH_2Cl_2 at −78 °C. 1,4-Phenylene diisocyanide was purchased from Aldrich and used as received.

Preparation of [*rac*-$Ph_2H_2C_2(\eta^5\text{-}C_5H_4)_2$}CrCN-*t*-Bu][$B(C_6F_5)_4$] ([2b][$B(C_6F_5)_4$]). Solutions of $[Ph_3C][B(C_6F_5)_4]$ (0.52 g, 0.56 mmol) in 30 mL of toluene and **2b** (0.23 g, 0.52 mmol) in 30 mL of toluene were combined in a round-bottom flask in the glovebox and stirred for 6 h. Upon standing for an hour unstirred, the reaction mixture separated into two distinct layers, a yellow layer atop a red oil. The yellow layer was removed with a pipet and the volatiles from the red oil were removed under reduced pressure with gentle heating, leaving a red solid, which was recrystallized from toluene by storing the solution for several days at −30 °C (yield: 0.31 g, 53%). IR (Nujol mull): 2139, 2199 cm^{-1} (ν NC). Anal. Calcd for $C_{53}H_{29}CrBF_{20}N$: C, 56.72; H, 2.58; N, 1.25. Found: C, 57.07; H, 2.61; N, 0.90. μ_{eff} = 1.8 μ_B (Evans NMR method).

Preparation of {$(CH_3)_4C_2(\eta^5\text{-}C_5H_4)_2$}CrCN($CH_2$-*p*-Tosyl) (3). Diethyl ether (50 mL) was transferred under vacuum into a flask containing **1a** (0.75 g, 2.6 mmol) and CN(CH_2-*p*-Tosyl) (0.51 g, 2.6 mmol) cooled at −78 °C. The reaction was allowed to warm gradually to room temperature. At room temperature, a rapid evolution of CO gas was observed. The reaction was stirred for an additional hour after all gas evolution had ceased. All volatiles were removed from the reaction product under reduced pressure, and the red-brown powder was washed with 25 mL of petroleum ether. Crystallization of the material from toluene at −30 °C afforded 0.75 g of **3** (yield: 63%) as brown plates. ^{1}H NMR (300 MHz, 298 K, C_6D_6): δ 8.01(d, $^3J_{HH}$ = 7.8 Hz, 2H, C_6H_4), 6.75 (d, $^3J_{HH}$ = 7.7 Hz, 2H, C_6H_4), 4.98 (m, 4H, C_5H_4), 4.53 (s, 2H, SCH_2), 3.97 (m, 4H, C_5H_4), 1.83 (s, 3H, $CH_3C_6H_4S$), 0.88 (s, 12H, $(CH_3)_4C_2$). ^{13}C{^{1}H} NMR (125 MHz, 298 K, C_6D_6): δ 290.6 (Cr*C*N), 144.1, 136.1, 129.4 128.3 (C_6H_4), 112.7, 81.4, 76.5 (C_5H_4), 71.4 ($NCCH_2S$), 44.3 ($C_2(CH_3)_4$), 27.1 (($CH_3)_4C_2$), 21.0 ($CH_3C_6H_4$). IR (Nujol mull): 1752 cm^{-1}; THF solution, 1774 cm^{-1} (ν CN). Anal. Calcd for $C_{25}H_{29}CrNO_2S$: C, 65.33; H, 6.37; N, 3.04. Found: C, 63.03; H, 6.31; N, 2.32. Carbon was consistently low upon reanalysis.

Preparation of {$(CH_3)_4C_2(\eta^5\text{-}C_5H_4)_2$}CrCN(Xyl) (4). The synthetic procedure is identical to that described for **3**. The reaction between **1a** (0.50 g, 1.7 mmol) and CNXyl (0.22 g, 1.7 mmol) afforded 0.45 g of **4** (72% yield) as orange plates. ^{1}H NMR (300 MHz, 298 K, C_6D_6): δ 6.90−6.80 (m, 3H, C_6H_3), 4.70 (m, 4H, C_5H_4), 3.84 (m, 4H, C_5H_4), 2.20 (s, 6H, 2,6-$(CH_3)_2C_6H_3$), 0.87 (s, 12H, $(CH_3)_4C_2$). ^{13}C{^{1}H} NMR (125 MHz, 298 K, C_6D_6): δ 239.7 (Cr*C*N), 134.7, 132.4, 128.4, 123.1 (C_6H_3), 108.4, 80.3, 75.3 (C_5H_4), 44.2 ($C_2(CH_3)_4$), 27.3 (($CH_3)_4C_2$), 18.5 (($CH_3)_2C_6H_3$). IR (Nujol mull): 2006 cm^{-1}; (THF) 1980 cm^{-1} (ν CN). Anal. Calcd for $C_{25}H_{29}CrN$: C, 75.92; H, 7.41; N, 3.53. Found: C, 74.76; H, 6.69; N, 3.31. Carbon was consistently low on reanalysis.

Preparation of [{$(CH_3)_4C_2(\eta^5\text{-}C_5H_4)_2$}CrCN(Xyl)][$B(C_6F_5)_4$] ([4][$B(C_6F_5)_4$]). The synthesis is the same as that described above for [**2b**$^+$][$B(C_6F_5)_4$]. The reaction between $[Ph_3C][B(C_6F_5)_4]$ (0.42 g, 0.46 mmol) and **4** (0.16 g, 0.40 mmol) in 30 mL of toluene afforded 0.24 g (49% yield) of the product as a red crystalline solid. IR (Nujol mull): 2119 cm^{-1} (ν NC). μ_{eff} = 1.9 μ_B (Evans NMR method). Anal. Calcd for $C_{56}H_{37}CrBF_{20}N$: C, 54.75; H, 2.73; N, 1.30. Found: C, 55.27; H, 3.21; N, 1.31.

Preparation of [*rac*-{$Ph_2H_2C_2(\eta^5\text{-}C_5H_4)_2$}CrCN-($\eta^5$-$C_5H_5$)Fe (5). The synthetic procedure is similar to the ones above except that the reaction between **1a** (0.99 g, 2.5 mmol) and isocyanoferrocene (0.46 g, 2.2 mmol) was performed in 50 mL of THF instead of Et_2O, and the reaction mixture was heated at 40 °C for 20 min. Removal of the solvent under reduced pressure left a reddish-brown solid consisting of **5** and a paramagnetic side product. Separation of **5** from the side product was achieved by extracting the solid with ca. 300 mL of Et_2O. Compound **5** precipitated upon reducing the volume of the ethyl ether extract to 30 mL under vacuum, and 0.67 g (54% yield) was isolated after filtration. Single crystals of **5** were obtained by slow evaporation of a solution of the compound in benzene-d_6 under a nitrogen atmosphere. ^{1}H NMR (300 MHz, 298 K, C_6D_6): δ 7.13 (m, 4H, C_6H_5), 7.07−7.00 (m, 6H, C_6H_5), 4.94 (m, 2H, $(C_5H_4)_2Cr$), 4.54 (m, 2H, $(C_5H_4)_2Cr$), 4.45 (m, 1H, CN(C_5H_4)Fe), 4.42 (m, 1H, NC-(C_5H_4)Fe), 4.26 (m, 2H, $(C_5H_4)_2Cr$), 4.17 (s, 5H, (C_5H_5)Fe), 3.90 (s, 2H, $Ph_2C_2H_2$), 3.91 (m, 2H, NC(C_5H_4)Fe), 3.87 (m, 2H, $(C_5H_4)_2$-Cr). ^{13}C{^{1}H} NMR (125 MHz, 298 K, C_6D_6): δ 274.0 (N*C*Cr), 126.7, 127.5, 128.3, 142.4 (C_6H_5), 82.0, 80.0, 78.6, 77.9 (($C_5H_4)_2$-Cr), 69.7 ((C_5H_5)Fe), 64.0, 65.9 ((CNC_5H_4)Fe), 54.8 ($Ph_2C_2H_2$). IR (Nujol mull): 1829 cm^{-1} (ν NC). Anal. Calcd for $C_{35}H_{29}CrFeN$: C, 73.56; H, 5.10; N, 2.45. Found: C, 73.95; H, 5.03; N, 2.52.

Preparation of [[*rac*-{$Ph_2H_2C_2(\eta^5\text{-}C_5H_4)_2$}CrCN-($\eta^5$-$C_5H_4$)]-($\eta^5$-$C_5H_5$)Fe][$PF_6$] ([5][$PF_6$]). Complex **5** was prepared in situ by reacting **1a** (800 mg, 2.1 mmol) with isocyanoferrocene (400 mg, 1.9 mmol) in 50 mL of THF. The solution was cooled to 0 °C, and $[(C_5H_5)_2Fe][PF_6]$ (626 mg, 1.9 mmol) was added via a solid dispenser sidearm. This mixture was stirred for 30 min at 0 °C under an atmosphere of argon. Cooling the solution to −78 °C produced a brown precipitate, which was collected by filtration to afford 0.91 mg of product (68% yield). ^{1}H NMR (300 MHz, 298 K, acetone-d_6): 7.88, 7.08 (broad, C_6H_5), 4.76 (broad, CN(C_5H_4)-Fe), 4.13 (broad, (C_5H_5)Fe), 3.27 (broad, CN(C_5H_4)Fe). ^{31}P NMR (202 MHz, 298 K, acetone-d_6): δ −142.7(hept., $^1J_{PF}$ = 707 Hz). ^{19}F NMR, (470 MHz, 298 K, acetone-d_6): δ −69.85 (d, $^1J_{PF}$ = 707 Hz). IR (Nujol mull): 2118 cm^{-1} (ν NC). Anal. Calcd for $C_{35}H_{29}CrFeNPF_6$: C, 59.06; H, 4.42; N, 1.86. Found: C, 59.12; H, 4.35; N, 1.66. μ_{eff} = 1.9 μ_B (magnetic susceptibility balance and Evans NMR method).

Preparation of 1,4-[$Me_2C_2(\eta^5\text{-}C_5H_4)_2$}CrCN]$_2C_6H_4$ (6). The synthetic procedure is similar to the one described for **5**. After heating the 50 mL THF solution of reactants **1a** (1.3 g, 4.6 mmol) and 1,4-phenylene diisocyanide (295 mg, 2.3 mmol) at 40 °C for 20 min, the solution was concentrated to 25 mL and cooled to −78 °C to afford crystals of deep red **6** (0.98 g, 65% yield), which were isolated by filtration. Single crystals of **6** were obtained by slow evaporation of a THF/C_6D_6 solution of the compound. ^{1}H NMR (500 MHz, 25 °C, C_6D_6): δ 7.53 (s, 4H, CNC_6H_4NC) 4.57 (m, 8H, $(C_5H_4)_2Cr$), 3.99 (m, 8H, $(C_5H_4)_2Cr$), 0.95 (s, 24H, $C_2(CH_3)_4$). ^{13}C NMR, (500 MHz, 25 °C, C_6D_6): δ 278.3 (N*C*), 124.7, 140.4 (CNC_6H_4NC), 76.2, 80.6, (($C_5H_4)_2Cr$), 44.5 ($C_2(CH_3)_4$), 27.4 (C_2-$(CH_3)_4$). IR (Nujol mull): 1766 cm^{-1} (ν NC)). Anal. Calcd for $C_{40}H_{44}Cr_2N_2$: C, 73.15; H, 6.75; N, 4.27. Found: C, 70.36; H, 6.37; N, 3.81. Carbon was consistently low on reanalysis.

Preparation of [1,4-[$Me_2C_2(\eta^5\text{-}C_5H_4)_2$}CrCN]$_2C_6H_4$][B(3,5-$(CF_3)_2C_6H_3)_4$]$_2$ ([6][$B(Ar_F)_4$]$_2$). A mixture of complex **6** (0.145 g, 0.22 mmol) and $[Cp_2Fe][B(Ar_F)_4]$ (0.462 g, 0.44 mmol) was dissolved in 30 mL of THF at −78 °C. The reaction mixture was allowed to warm to 0 °C and stirred for 45 min. The solvent of the resulting dark brown solution was removed under vacuum, and the residue was washed with warm benzene (4 × 15 mL) to remove the ferrocene coproduct. The red-brown powder was dissolved in methylene chloride, and the solution was filtered and then concentrated to 15 mL and stored for 20 h at −35 °C, forming large, brown crystals, which were isolated by filtration and dried under vaccum, affording 0.365 g of $\mathbf{6}^{2+}$ (70% yield). ^{1}H NMR (300 MHz, 298 K, DMSO-d_6): δ 7.71 (s, 8H, $B(Ar_F)_4$ *p-H*), 7.60 (s, 16H, $B(Ar_F)_4$ *o-H*), −2.16 (bs, $C_2(CH_3)_4$). ^{19}F NMR (280 MHz, DMSO-d_6): δ −61.58 (s, CF_3). IR (Nujol mull): 2088 cm^{-1} (ν CN). μ_{eff} = 2.3 μ_B (magnetic susceptibility balance and Evans NMR method). The molecule cocrystallized with 0.225 equiv of CH_2Cl_2. Anal. Calcd for $C_{104.225}H_{68.500}B_2Cl_{0.500}F_{48}N_2Cr_2$: C, 52.11; H, 2.87; N, 1.17. Found: C, 51.72; H, 3.08; N, 1.21.

(47) Heinekey, D. M.; Radzewich, C. E. *Organometallics* **1988**, *7*, 51−58.

Preparation of [$Me_2C_2(\eta^5$-$C_5H_4)_2$}CrCN-(η^5-C_5H_4)]$_2$Fe (7a). The synthetic procedure is similar to the one described for **5**. After heating the 50 mL THF solution of reactants **1a** (1.0 g, 3.4 mmol) and diisocyanoferrocene (0.40 g, 1.7 mmol) at 40 °C for 20 min, the solution was concentrated to 20 mL and 60 mL of hexane was layered on top of the solution. The reddish-brown product was crystallized by cooling this mixture at −78 °C, and 0.64 g (49% yield) was collected by cold filtration. Single crystals of **7a** were obtained by slow evaporation of a solution of the compound in C_6D_6. ^{1}H NMR (500 MHz, 298 K, THF-d_8): δ 4.76 (m, 8H, (C_5H_4)-Cr), 4.30 (m, 4H, (C_5H_4)Fe), 4.04 (m, 4H, (C_5H_4)Fe) 3.92 (m, 8H, (C_5H_4)Cr), 1.19 (s, 24H, $C_2(CH_3)_4$). ^{13}C{^{1}H} NMR (125 MHz, 298 K, C_6D_6): δ 278.6 (N*C*Cr), 80.8, 76.1, (*C*$_5$H$_4$)Cr), 65.2, 66.8, ((*C*$_5$H$_4$)Fe), 44.5 (*C*$_2$(CH$_3$)$_4$), 27.5 (C$_2$(*C*H$_3$)$_4$). IR (Nujol mull): 1751 cm^{-1} (ν NC). Anal. Calcd for $C_{50}H_{54}Cr_2FeN_2$: C, 69.1; H, 6.37; N, 3.63. Found: C, 68.72; H, 6.21; N, 3.49.

Preparation of [*rac*-$Ph_2H_2C_2(\eta^5$-$C_5H_4)_2$}CrCN-(η^5-C_5H_4)]$_2$Fe (7b). The synthetic procedure is similar to the one described for **5**. After heating the 50 mL THF solution of reactants **1b** (1.0 g, 2.6 mmol) and diisocyanoferrocene (0.30 g, 1.3 mmol) at 40 °C for 20 min, the volatiles were removed under reduced pressure and the product was extracted from the reddish-brown residue with 300 mL of ethyl ether. The product was precipitated by concentrating the ether solution to 30 mL and was collected by filtration (0.78 g, 63% yield). ^{1}H NMR (500 MHz, 298 K, THF-d_8): δ 7.08, 7.16, 7.28 (m, 20H, C$_6$H$_5$), 5.30 (m, 4H, (C$_5$H$_4$)Cr), 4.75 (m, 4H, (C$_5$H$_4$)-Cr), 4.43 (m, 1H, (C$_5$H$_4$)Fe), 4.41 (m, 2H, (C$_5$H$_4$)Fe), 4.38 (m, 1H, (C$_5$H$_4$)Fe), 4.27 (m 4H, (C$_5$H$_4$)Cr), 4.20 (s, 4H, [Ph$_2$C$_2$H$_2$]), 4.12 (m, 4H, (C$_5$H$_4$)Fe), 3.86 (m, 4H, (C$_5$H$_4$)Cr). ^{13}C NMR, (125 MHz, 298 K, THF-d_8): δ 276.2 (N*C*Cr). 127.2, 128.5, 128.9, 143.7 (*C*$_6$H$_5$), 82.6, 82.5, 80.5, 79.1, 78.1, ((*C*$_5$H$_4$)Cr), 67.0 65.4, 65.3, 65.2, (*C*$_5$H$_4$)Fe), 55.3 (Ph$_2$*C*$_2$H$_2$). IR (Nujol mull): 1763 cm^{-1} (ν NC). Anal. Calcd for $C_{60}H_{48}Cr_2FeN_2$: C, 75.31; H, 5.06; N, 2.93. Found: C, 73.95; H, 5.03; N, 2.52. Carbon was consistently low on reanalysis.

Preparation of [[*rac*-$Ph_2H_2C_2(\eta^5$-$C_5H_4)_2$}CrCN-(η^5-C_5H_4)]$_2$Fe]-[PF_6]$_2$ ([7b][PF_6]$_2$). The same procedure as described for **[5][PF_6]** was used. Complex **7b** was formed in situ from **1b** (0.90 g, 2.3 mmol) and diisocyanoferrocene (0.27 g,1.16 mmol) in 50 mL of THF and reacted with [(C$_5$H$_5$)$_2$Fe][PF$_6$] (0.77 g, 2.3 mmol) at 0 °C. The product was precipitated from solution at −78 °C and collected by filtration, affording 0.95 g of **[7b][PF_6]$_2$** (65% yield). ^{1}H NMR (300 MHz, 298 K, acetone-d_6): δ 8.03 (broad, C$_6$H$_5$). 7.37 (broad, C$_6$H$_5$), 7.07 (broad, C$_6$H$_5$), 4.96 (broad, CN(C$_5$H$_4$)-Fe), 3.13 (broad, CN(C$_5$H$_4$)Fe). ^{31}P NMR, (202 MHz, 298 K, acetone-d_6): δ −142.2 hept., $^1J_{PF}$ = 707 Hz). ^{19}F NMR (470 MHz, 25 °C, acetone-d_6): δ −69.83 (d, $^1J_{PF}$ = 707 Hz). IR (Nujol mull): 2113 cm^{-1} (free diisocyanoferrocene), 2137 cm^{-1} (ν NC). μ_{eff} = 2.6 μ_B (magnetic susceptibility balance and Evans NMR method). Anal. Calcd for $C_{60}H_{48}Cr_2FeN_2P_2F_{12}$: C, 57.80; H, 3.88; N, 2.25. Found: C, 54.98; H, 3.84; N, 2.21. Carbon was consistently low on reanalysis. The IR band for free diisocyanoferrocene at 2113 cm^{-1} indicates that this ligand dissociates readily from the complex. Partial ligand loss during purification could account for the low carbon value, as could incomplete combustion.

X-ray Structure Determinations. Crystals of each compound were removed from the flask and covered with a layer of hydrocarbon oil. A suitable crystal was selected from each, attached to a glass fiber, and placed in the low-temperature nitrogen stream.[48] Data for **2**, **[2b][B(C$_6$F$_5$)$_4$]**, **[4][B(C$_6$F$_5$)$_4$]**, and **5** were collected at 203(2) K using a Bruker/Siemens SMART 1K and Siemens LT-2A low-temperature device; **3**, **4** at 203(2) K (LT-2A) and **6**, **7b** at 81(2) K using a Bruker APEX instrument and a Cryocool NeverIce low-temperature device. Data were measured with Mo Kα radiation (λ = 0.71073 Å) using omega scans of 0.3° per frame for **2** (40 s, 1471 frames); **[2b][B(C$_6$F$_5$)$_4$]** (20 s, 2132 frames); **3** (20 s, 2132 frames); **4** (30 s, 1471 frames); **[4][B(C$_6$F$_5$)$_4$]** (20 s, 1471 frames); **5** (20 s, 1471 frames); **6** (40 s, 1471 frames); **7a** (5 s, 2132 frames). The first 50 frames were re-collected at the end of data collection to monitor for decay. Cell parameters were retrieved using SMART[49] software and refined using SAINTPlus[50] on all observed reflections. Data reduction and correction for *Lp* and decay were performed using the SAINTPlus software. Absorption corrections were applied using SADABS.[51] The structure was solved by direct methods and refined by least-squares method on F^2 using the SHELXTL program package.[52] All non-hydrogen atoms were refined anisotropically except for **[2b][B(C$_6$F$_5$)$_4$]**. In this compound, the *ansa* backbone and phenyl are disordered over two positions (60% major fraction). The disordered carbon atoms were held isotropic. No decomposition was observed during data collection. Details of the data collection and refinement are given in Table 1.

Calculations. All calculations were carried out with the Turbomole program[53,54] coupled to the PQS Baker optimizer.[55,56] Calculations on open-shell systems used the spin-unrestricted formalism. Geometries were optimized without constraints at the bp86[57,58]/RIDFT[59] level using the Turbomole SV(P) basis set[53,60] on all atoms. Improved energies were obtained from single-point calculations at the b3-lyp level[61−64] using the TZVP basis.[53,65] Solvent corrections were calculated at the b3-lyp/TZVP level using the COSMO solvation model[66] with a dielectric constant of 7.5 (THF). For these relatively large systems, vibrational analyses (and hence thermal corrections) were not feasible.

CCDC 265602−265609 contain the supplementary crystallographic data for this paper. These data can be obtained free of charge via www.ccdc.cam.ac.uk/data_request/cif, by e-mailing data_request@ccdc.cam.ac.uk, or by contacting The Cambridge Crystallographic Data Centre, 12 Union Road, Cambridge CB2 1EZ, UK; fax: +44 1223 336033.

Acknowledgment. The authors are grateful to the donors of the Petroleum Research Fund, administered by the American Chemical Society, the National Science Foundation (grant no.

(48) Hope, H. *Prog. Inorg. Chem.* **1995**, *41*, 1−19.

(49) *SMART*: Bruker Molecular Analysis Research Tool; Bruker AXS: Madison, WI, 2002.

(50) *SAINTPlus*: Data Reduction and Correction Program; Bruker AXS: Madison, WI, 2001.

(51) *SADABS*: an empirical absorption correction program; Bruker AXS Inc.: Madison, WI, 2001.

(52) Sheldrick, G. M. *SHELXTL*: Structure Determination Software Suite; Bruker AXS Inc.: Madison, WI, 2001.

(53) Ahlrichs, R.; Bär, M.; Baron, H.-P.; Bauernschmitt, R.; Böcker, S.; Ehrig, M.; Eichkorn, K.; Elliott, S.; Furche, F.; Haase, F.; Häser, M.; Hättig, C.; Horn, H.; Huber, C.; Huniar, U.; Kattannek, M.; Köhn, A.; Kölmel, C.; Kollwitz, M.; May, K.; Ochsenfeld, C.; Öhm, H.; Schäfer, A.; Schneider, U.; Treutler, O.; Tsereteli, K.; Unterreiner, B.; von Arnim, M.; Weigend, F.; Weis, P.; Weiss, H. *Turbomole* Version 5; Theoretical Chemistry Group, University of Karlsruhe, January 2002.

(54) Treutler, O.; Ahlrichs, R. *J. Chem. Phys.* **1995**, *102*, 346−354.

(55) *PQS* version 2.4; Parallel Quantum Solutions: Fayetteville, AK, 2001 (the Baker optimizer is available separately from PQS upon request).

(56) Baker, J. *J. Comput. Chem.* **1986**, *7*, 385−395.

(57) Becke, A. D. *Phys. Rev. A* **1988**, *38*, 3098−3100.

(58) Perdew, J. P. *Phys. Rev. B* **1986**, *33*, 8822−8824.

(59) Eichkorn, K.; Weigend, F.; Treutler, O.; Ahlrichs, R. *Theor. Chem. Acc.* **1997**, *97*, 119−124.

(60) Schäfer, A.; Horn, H.; Ahlrichs, R. *J. Chem. Phys.* **1992**, *97*, 2571−2577.

(61) Lee, C.; Yang, W.; Parr, R. G. *Phys. Rev. B* **1988**, *37*, 785−789.

(62) Becke, A. D. *J. Chem. Phys.* **1993**, *98*, 1372−1377.

(63) Becke, A. D. *J. Chem. Phys.* **1993**, *98*, 5648−5652.

(64) All calculations were performed using the Turbomole functional "b3-lyp", which is not identical to the Gaussian "B3LYP" functional.

(65) Schäfer, A.; Huber, C.; Ahlrichs, R. *J. Chem. Phys.* **1994**, *100*, 5829−5835.

(66) Klamt, A.; Schürmann, G. *J. Chem. Soc., Perkin Trans. 2* **1993**, 799−805.

CHE-9816730), and the Department of Energy (grant no. DE-FG0298ER45709) for their generous financial support. The establishment of a Single-Crystal X-ray Diffraction Laboratory and the purchase of a 500 MHz NMR spectrometer were supported by the M. J. Murdock Charitable Trust of Vancouver, WA, the National Science Foundation, and the NSF Idaho EPSCoR Program.

Supporting Information Available: CIF files with X-ray crystallographic information for compounds **2a**, **[2b][B(C_6F_5)$_4$]**, **3**, **4**, **[4][B(C_6F_5)$_4$]**, **5**, **6**, and **7a** and ^{1}H NMR spectra for compounds **3**, **4**, **6**, and **7b**. This material is available free of charge via the Internet at http://pubs.acs.org.

OM050710J